ance by interferon therapy.[11] The present *in vivo* findings also showed that increased *SOCS3* expression in the liver prior to interferon treatment impaired the phosphorylation of STAT1 and that the area immunostaining to *SOCS3* was an important factor for predicting HCV clearance by interferon therapy.

In this study, area immunostaining to *SOCS3* was significantly correlated with HOMA-IR. Because the liver is the primary site of insulin resistance, insulin resistance caused by increased hepatic expression of *SOCS3* protein may lead to persistent hyperinsulinemia that further exacerbates insulin resistance.[17,18] Recent data indicate that the incidence of altered baseline glucose level and the frequency of diabetes type 2 were greater in non-responder cases than in SVR cases.[19] Experimental data obtained using the replicon model also indicate that when an insulin level similar to that seen clinically in hyperinsulinemia was added to interferon, the ability to block HCV replication disappeared.[20] Taken together, these findings show that insulin signaling is associated with interferon signaling. Our data suggest that one factor important in the association between insulin signaling and interferon signaling is *SOCS3*.

SOCS3 immunostaining was mainly seen in the periportal area. *SOCS3* is induced by proinflammatory stimuli such as TNF-α and LPS,[12,21] indicating that these proinflammatory stimuli may enhance *SOCS3* expression via portal vein flow. Adipocytokines such as TNF-α induced by visceral fat have been shown to cause insulin resistance by increasing serine phosphorylation of insulin receptor substrate (IRS)-1.[22,23] On basis of these data, these adipocytokines are likely to enhance *SOCS3* expression and induce both insulin resistance and interferon resistance.

SOCS3 immunostaining score was observed to significantly correlate with AST and ALT and was significantly higher in patients with severe inflammation than in those with mild inflammation. This finding was consistent with previous reports that *SOCS3* expression is influenced by inflammatory state.[24,25]

Moreover, *SOCS3* immunostaining score was negatively correlated with platelet count and was also significantly higher in patients with severe fibrosis than in those with mild fibrosis. *SOCS3* is known to act as a negative regulator in hepatocyte proliferation, and the progression of fibrosis is associated with reduced cellular proliferation.[26,27] Our results showed that *SOCS3* expression increased and liver regeneration was impaired during the progression of liver fibrosis.

In this study, 14 patients were younger than 60 and had *SOCS3* immunostaining of < 30% of specimen area. These 14 patients all demonstrated SVR. Specificity of the combination of *SOCS3* and age was 100%. Therefore, prior to interferon therapy, consideration of age and quantification of the area immunostaining to *SOCS3* on hepatic biopsy can be considered simple and useful for predicting a positive response to interferon. Some previous study also reported that *SOCS3* expression was a factor associated with response to treatment.[15,16] Most of previous study was subjected to Caucasoid, few study subjected to Asian patients. Our study showed that immunostaing of *SOCS3* in the liver also significant predictor of HCV clearance by interferon therapy in Asian patients. Recently, Persico *et al.* reported that the *SOCS3* -4874 AA genotype was strongly associated with failure of antiviral therapy, and that the AA genotype carriers had significantly higher *SOCS3* mRNA and protein levels,[28] suggesting that the high expression of *SOCS3* in the liver tissue, which we observed in non-SVR patients, may be related to *SOCS3* -4874 AA genotype. Further study is needed to confirm this.

In conclusion, response to antiviral therapy may be conditioned by *SOCS3* expression. Moreover, expression of *SOCS3* was influenced by insulin resistance. Taken together, a good response to interferon therapy is needed for improvement in insulin resistance.

SOCS3 expression in the liver prior to interferon therapy was correlated with increased insulin resistance and might be a useful predictor of HCV clearance by interferon therapy.

REFERENCES

1 Mangia A, Ricci GL, Persico M *et al.* A randomized controlled trial of pegylated interferon alpha-2a (40 KD) or interferon alpha-2a plus ribavirin and amantadine vs interferon alpha-2a and ribavirin in treatment-naive patients with chronic hepatitis C. *J Viral Hepat* 2005; **12**: 292–9.

2 Akuta N, Suzuki F, Kawamura Y *et al.* Predictive factors of early and sustained responses to peginterferon plus ribavirin combination therapy in Japanese patients infected with hepatitis C virus genotype 1b: amino acid substitutions in the core region and low-density lipoprotein cholesterol levels. *J Hepatol* 2007; **46**: 403–10.

3 Wedemeyer H, Wiegand J, Cornberg M *et al.* Polyethylene glycol-interferon: Current status in hepatitis C virus therapy. *J Gastroenterol Hepatol* 2002; **17** (Suppl 3): S344–S350.

4 Davis GL, Esteban-Mur R, Rustgi V *et al.* Interferon alfa-2b alone or in combination with ribavirin for the treatment of relapse of chronic hepatitis C. International Hepatitis Interventional Therapy Group. *N Engl J Med* 1998; **339**: 1493–9.

5 Poynard T, Marcellin P, Lee SS *et al.* Randomised trial of interferon alpha2b plus ribavirin for 48 weeks or for 24 weeks versus interferon alpha2b plus placebo for 48 weeks for treatment of chronic infection with hepatitis C virus. International Hepatitis Interventional Therapy Group (IHIT). *Lancet* 1998; 352: 1426–32.
6 Yang CH, Murti A, Pfeffer LM STAT3 complements defects in an interferon-resistant cell line: evidence for an essential role for STAT3 in interferon signaling and biological activities. *Proc Natl Acad Sci USA* 1998; 95: 5568–72.
7 Jacoby JJ, Kalinowski A, Liu MG *et al.* Cardiomyocyte-restricted knockout of STAT3 results in higher sensitivity to inflammation, cardiac fibrosis, and heart failure with advanced age. *Proc Natl Acad Sci USA* 2003; 100: 12929–34.
8 Williams L, Bradley L, Smith A *et al.* Signal transducer and activator of transcription 3 is the dominant mediator of the anti-inflammatory effects of IL-10 in human macrophages. *J Immunol* 2004; 172: 567–76.
9 Klein C, Wustefeld T, Assmus U *et al.* The IL-6-gp130-STAT3 pathway in hepatocytes triggers liver protection in T cell-mediated liver injury. *J Clin Invest* 2005; 115: 860–9.
10 Taub R. Hepatoprotection via the IL-6/Stat3 pathway. *J Clin Invest* 2003; 112: 978–80.
11 Miyaaki H, Ichikawa T, Nakao K *et al.* Predictive value of phosphorylation of signal transducers and activators of transcription in the outcome of interferon therapy for chronic hepatitis C. *Intervirlogy* 2008; 51 (6): 394–9.
12 Bode JG, Ludwig S, Ehrhardt C *et al.* IFN-alpha antagonistic activity of HCV core protein involves induction of suppressor of cytokine signaling-3. *FASEB J* 2003; 17: 488–90.
13 Kawaguchi T, Yoshida T, Harada M *et al.* Hepatitis C virus down-regulates insulin receptor substrates 1 and 2 through up-regulation of suppressor of cytokine signaling 3. *Am J Pathol* 2004; 165: 1499–508.
14 Yasukawa H, Sasaki A, Yoshimura A. Negative regulation of cytokine signaling pathways. *Annu Rev Immunol* 2000; 18: 143–64.
15 Persico M, Capasso M, Persico E *et al.* Suppressor of cytokine signaling 3 (*SOCS3*) expression and hepatitis C virus-related chronic hepatitis: Insulin resistance and response to antiviral therapy. *Hepatology* 2007; 46: 1009–15.
16 Huang Y, Feld JJ, Sapp RK *et al.* Defective hepatic response to interferon and activation of suppressor of cytokine signaling 3 in chronic hepatitis C. *Gastroenterology* 2007; 132: 733–44.
17 Michael MD, Kulkarni RN, Postic C *et al.* Loss of insulin signaling in hepatocytes leads to severe insulin resistance and progressive hepatic dysfunction. *Mol Cell* 2000; 6: 87–97.
18 Poy MN, Yang Y, Rezaei K *et al.* CEACAM1 regulates insulin clearance in liver. *Nat Genet* 2002; 30: 270–6.
19 Konishi I, Horiike N, Hiasa Y *et al.* Diabetes mellitus reduces the therapeutic effectiveness of interferon-alpha2b plus ribavirin therapy in patients with chronic hepatitis C. *Hepatol Res* 2007; 37: 331–6.
20 Romero-Gomez M. Insulin resistance and hepatitis C. *World J Gastroenterol* 2006; 12: 7075–80.
21 Ehlting C, Lai WS, Schaper F *et al.* Regulation of suppressor of cytokine signaling 3 (*SOCS3*) mRNA stability by TNF-alpha involves activation of the MKK6/p38MAPK/MK2 cascade. *J Immunol* 2007; 178: 2813–26.
22 Bode JG, Nimmesgern A, Schmitz J *et al.* LPS and TNFalpha induce *SOCS3* mRNA and inhibit IL-6-induced activation of STAT3 in macrophages. *FEBS Lett* 1999; 463: 365–70.
23 Hotamisligil GS, Peraldi P, Budavari A *et al.* IRS-1-mediated inhibition of insulin receptor tyrosine kinase activity in TNF-alpha- and obesity-induced insulin resistance. *Science* 1996; 271: 665–8.
24 Jo D, Liu D, Yao S *et al.* Intracellular protein therapy with *SOCS3* inhibits inflammation and apoptosis. *Nat Med* 2005; 11: 892–8.
25 Yang XP, Schaper F, Teubner A *et al.* Interleukin-6 plays a crucial role in the hepatic expression of *SOCS3* during acute inflammatory processes *in vivo*. *J Hepatol* 2005; 43: 704–10.
26 Cressman DE, Greenbaum LE, DeAngelis RA *et al.* Liver failure and defective hepatocyte regeneration in interleukin-6-deficient mice. *Science* 1996; 274: 1379–83.
27 Li W, Liang X, Kellendonk C *et al.* STAT3 contributes to the mitogenic response of hepatocytes during liver regeneration. *J Biol Chem* 2002; 277: 28411–7.
28 Persico M, Capasso M, Russo R *et al.* Elevated expression and polymorphisms of *SOCS3* influence patient response to antiviral therapy in chronic hepatitis C. *Gut* 2008; 57: 507–15.

A high glucose condition sensitizes human hepatocytes to hydrogen peroxide-induced cell death

HIDETAKA SHIBATA[1], TATSUKI ICHIKAWA[1], KAZUHIKO NAKAO[1], HISAMITSU MIYAAKI[1], SHIGEYUKI TAKESHITA[1], MOTOHISA AKIYAMA[1], MASUMI FUJIMOTO[1], SATOSHI MIUMA[1], SHOUGO KANDA[2], HIRONORI YAMASAKI[3] and KATSUMI EGUCHI[1]

[1]The First Department of Internal Medicine, [2]Department of Clinical Pharmaceutics, and [3]Health Research Center, Graduate School of Biomedical Sciences, Nagasaki University, Nagasaki, Japan

Received December 27, 2007; Accepted February 13, 2008

Abstract. Oxidative stress is known to play a key role in the progression of liver disease, including non-alcoholic steatohepatitis (NASH), which is often accompanied by hyperglycemia. This study examined the influence of high glucose on oxidative stress-induced hepatic cell death. Hc cells, a normal human hepatocyte-derived cell line, were cultured in normal-to-high glucose (5.5-22 mM)-containing medium with varying concentrations (0.01-1 mM) of hydrogen peroxide. In certain experiments, cyclosporine A (CyA), which inhibits the mitochondrial permeability transition (MPT) pore, or Z-VAD-FMK (z-VAD), a pan-caspase inhibitor, were added to the medium. Cell viability was evaluated using a colorimetric assay. The mode of cell death was determined by nuclear staining methods using Hoechst 33258 and Sytox green. Neither high glucose (22 mM) nor 0.05-0.5 mM of hydrogen peroxide alone killed Hc cells. However, a combination of the two induced cell death, causing the nuclei of Hc cells to become expanded rather than condensed, and the nuclear membrane to become weak. CyA, but not z-VAD, blocked cell death. These results suggest that a high glucose condition may cause human hepatocytes to undergo hydrogen peroxide-induced necrotic cell death.

Correspondence to: Dr Tatsuki Ichikawa, The First Department of Internal Medicine, Graduate School of Biomedical Sciences, Nagasaki University, 1-7-1 Sakamoto, Nagasaki 852-8501, Japan
E-mail: ichikawa@nagasaki-u.ac.jp

Abbreviations: NASH, non-alcoholic steatohepatitis; ALD, alcoholic liver disease; HCV, hepatitis C virus; ROS, reactive oxygen species; CTGF, connective tissue growth factor; CyA, cyclosporine A; MPT, mitochondrial permeability transition; CypD, cyclophilin D; Tac, tacrolimus

Key words: high glucose, reactive oxygen species, hepatocyte cell death, necrosis, cyclosporine A

Introduction

Recently, oxidative stress has been recognized as the major cause of liver disease, including non-alcoholic steatohepatitis (NASH), alcoholic liver disease (ALD) and hepatitis C virus (HCV)-related liver disease (1). The pathogenesis of oxidative stress is currently under investigation. Reactive oxygen species such as (ROS), superoxide and hydrogen peroxide, which are induced in the normal liver, are among the causes of oxidative stress. During inflammation due to infection, activated macrophages and neutrophils undergo respiratory bursts and release ROS to destroy invading organisms (2,3). This function is an important normal immune reaction to infection in the liver. Alcohol also causes increased ROS production in the liver through several metabolic pathways, and the induced ROS accelerate hepatocyte cell death (4,5). In addition, metabolic syndrome, closely associated with NASH, generates ROS in the liver and other tissues (6). ROS generation resulting in abnormal mitochondrial function has been observed in NASH, and oxidative stress plays a role not only in hepatic steatosis but also in hepatic fibrosis (7). HCV also causes mitochondrial damage in hepatocytes and increases ROS (8,9), followed by ROS-induced hepatic steatosis (10,11). Hepatic cancer in HCV transgenic mice is moreover associated with the generation of ROS (12). In short, ROS are generated with various liver diseases and influence hepatocyte and hepatic stromal cells (13). Oxidative stress has potentially important implications for the progression of liver disease.

Oxidative stress induces insulin resistance in the liver (14) and muscle (15). It is known that insulin resistance in the liver is brought on by deficiencies in insulin signaling in hepatocytes (16) and causes hyperinsulinemia, hyperglycemia and other metabolic syndrome factors. Both hyperinsulinemia and hyperglycemia were recently noted as being a cause of liver damage (17). A previous study revealed that maintaining normoglycemia by the use of insulin reduces morbidity and mortality in critically ill patients. This phenomenon is assumed to be related to the protection of hepatocyte mitochondria ultrastructure and function by normoglycemia (18). On the other hand, hyperglycemia-related cell death is observed in various cell types. For instance, high glucose has been reported to induce endothelial cell death (19), cardiac myoblast cell death

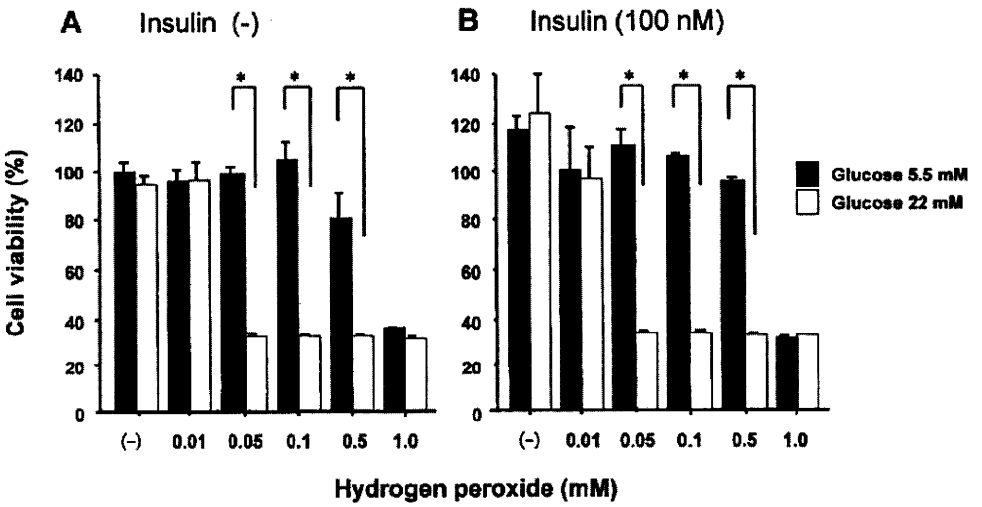

Figure 1. Effect of varying concentrations of hydrogen peroxide on Hc cell viability under normal or high glucose culture conditions in the absence (A) or presence (B) of insulin. Black bars indicate a normal glucose (5.5 mM) culture condition, and white bars a high glucose (22 mM) culture condition. After a 2-h exposure to hydrogen peroxide (0.01-1.0 mM), cell viability was determined using a colorimetric method. Cell viability in each culture condition is expressed as a percentage compared to the viability of the control (normal glucose medium without hydrogen peroxide and insulin). Data represent the mean ± SD values of four independent experiments. *p<0.01.

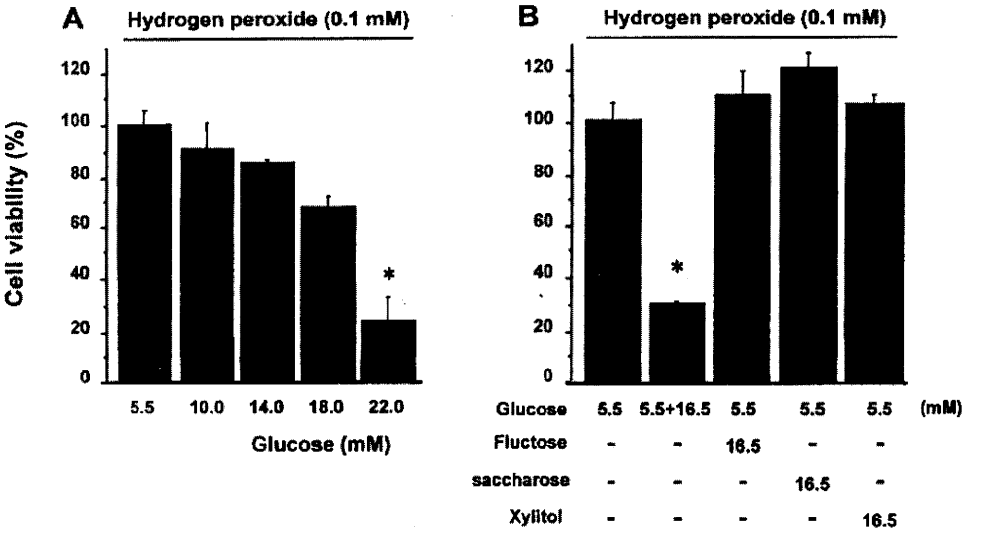

Figure 2. Effect of varying concentrations of glucose (A) and various types of saccharides (B) on hydrogen peroxide-induced Hc cell death. Hc cells were cultured in medium containing indicated concentrations of glucose with 0.1 mM hydrogen peroxide (A). Glucose, fructose, saccharose or xylitol (17.5 mM) were added to the culture medium containing 5.5 mM glucose with 0.1 mM hydrogen peroxide (B). Cell viability in each culture condition is expressed as a percentage compared to the viability of the control (5.5 mM glucose medium with 0.1 mM hydrogen peroxide). Data represent the mean ± SD values of four independent experiments. *p<0.01 vs. others.

(20), neuron death (21), muscle cell death (22) and podocyte cell death *in vitro* (23). In addition, high glucose stimulated connective tissue growth factor expression, a key factor of hepatic fibrosis, in hepatic stellate cells (24). This indicates that it might play an important role in hepatic fibrosis (25). However, the influence of high glucose on hepatocytes has not been thoroughly investigated.

Advanced liver disease by alcohol, NASH or HCV infection does not result from a single factor. The two-hit theory for the progression of NASH is a well-known hypothesis (26). Specifically, hepatic steatosis, which is correlated with oxidative stress caused by various etiologies (28), is known to be a co-factor in other liver diseases (27). A previous report demonstrated that ROS determines susceptibility to TGF-ß-induced apoptosis in cirrhotic hepatocytes (29) and to TNF-α-induced apoptosis in primary hepatocytes (30). Components of metabolic syndrome, such as hyperglycemia and hyperinsulinemia, may also be negative factors for liver disease (31,32). However, the influence of the combination of metabolic syndrome and ROS on hepatocyte cell death has yet to be examined.

This study attempted to examine the influence of high glucose on ROS-induced hepatocyte cell death using hydrogen peroxide as a representative ROS.

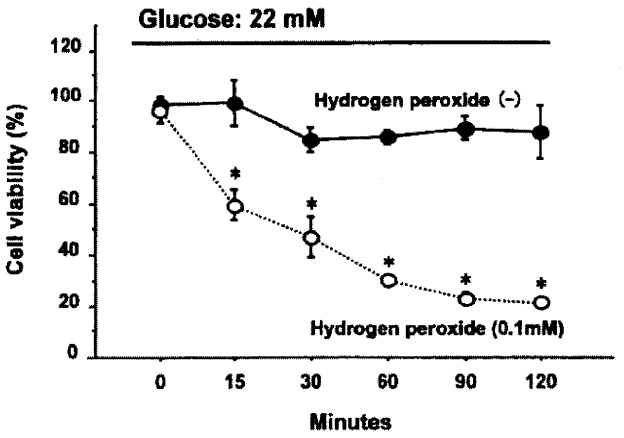

Figure 3. Time course of cell viability after exposure to high glucose with or without hydrogen peroxide. White circles indicate exposure with 0.1 mM hydrogen peroxide, and black circles exposure without hydrogen peroxide. Cell viability is expressed as a percentage compared to the viability of the control (22 mM glucose without 0.1 mM hydrogen peroxide at 0 min). Data represent the mean ± SD values of four independent experiments. *p<0.01 vs. without hydrogen peroxide at each indicated time point.

Materials and methods

Reagents and cell culture. Insulin, cyclosporine A (CyA) and tacrolimus (Tac) were generous gifts from Novartis Pharma Co. (Basel, Switzerland) and Astellas Co. (Tokyo, Japan), respectively. Z-VAD-FMK (z-VAD), a pan-caspase inhibitor, was purchased from Sigma (St. Louis, MO, USA), and hydrogen peroxide, fructose, saccharose and xylitol from Wako Pure Chemical Industries, Ltd. (Osaka, Japan).

Hc cells, a normal human hepatocyte-derived cell line, (Applied Cell Biology Research Institute, Kirkland, WA, USA) were maintained in Dulbecco's modified Eagle's medium (DMEM; Sigma) containing 5.5 mM glucose supplemented with 10% fetal bovine serum. Cells ($3x10^3$) were placed into 96-well multiplates. After 8 h, the medium was replaced with fresh serum-free DMEM containing 5.5 mM of glucose, and the cells were incubated for 24 h. This was followed by treatment with varying concentrations of hydrogen peroxide in serum-free DMEM containing 5.5 mM (normal) or 22 mM (high) glucose for 15-120 min. Next, cell viability was determined. In certain experiments, 100 nM of insulin was added to the culture medium together with hydrogen peroxide. Varying concentrations of CyA, Tac or z-VAD were added to the culture medium 30 min before hydrogen peroxide treatment.

Cell viability assay. Cell viability was determined by the colorimetric method using a Cell Counting Kit (Wako Life Science, Osaka, Japan). The absorbance of each well was measured at 405 nm with a microtiter plate reader (Multiskan JX, Thermo BioAnalysis Co., Japan). Data were expressed as the mean ± SD. Statistical significance was assessed using the Student's t-test. Statistically significant difference was defined as $p<0.05$. All numerical results are the mean of four independent experiments.

Fluorescent nuclear staining. The Hc cells were seeded onto 11-mm glass cover-slips in 24-well plates at $2x10^4$ cells/well. The next day, the medium was replaced with serum-free high or normal glucose DMEM, and the cells were treated with hydrogen peroxide. To determine the mode of cell death, Hc cells were incubated for 15 min with Sytox green nucleic acid stain (Molecular Probes, Eugene, OR, USA), which penetrates cells with compromised plasma membranes but does not cross the membranes of viable cells or apoptotic bodies. Hc cells were also stained with 1 mM of Hoechst 33258 (Invitrogen Japan K.K., Tokyo, Japan) for 30 min, and morphological changes in the nuclei were examined. Fluorescent nuclei were visualized using an Olympus BX50 microscope (Olympus, Tokyo, Japan) at 450-490 nm, and images captured using a Nikon DXM 1200 digital camera (Nikon, Tokyo, Japan).

Results

High glucose enhances sensitivity in hydrogen peroxide-induced Hc cell death. We examined the effects of a high glucose (22 mM) culture condition on the susceptibility of Hc cells to hydrogen peroxide (Fig. 1A). In normal glucose (5.5 mM) culture conditions, 0.05-0.5 mM hydrogen peroxide did not affect the viability of Hc cells. However, in high glucose (22 mM) culture conditions, Hc cells became susceptible to 0.05-0.5 mM hydrogen peroxide. Hydrogen peroxide (1 mM) killed Hc cells regardless of glucose concentrations. Since insulin stimulates the uptake and metabolism of glucose in cells, we added 100 nM insulin to the culture medium together with hydrogen peroxide (Fig. 1B). Although insulin seemed to increase cell viability in the absence of hydrogen peroxide, it could not restore the cell death induced by 0.05-0.5 mM hydrogen peroxide in a high glucose culture condition.

Effect of glucose on Hc cell death is dose dependent; other saccharides do not have a glucose-like effect at comparable concentrations. The relationship between hydrogen peroxide-induced Hc cell death and glucose concentrations in the culture medium was examined (Fig. 2A). With 0.1 mM of hydrogen peroxide, Hc cell viability decreased in higher glucose conditions compared to a normal glucose (5.5 mM) condition, and considerable cell death was detected in the highest glucose conditions (22 mM). There was a statistically significant difference between 22 mM glucose and the other glucose concentrations ($p<0.01$). To ascertain whether this phenomenon was due to a specific effect of glucose or to non-specific effects of high concentrations of saccharides, cell viability with exposure to 0.1 mM hydrogen peroxide was compared among similar concentrations of four different saccharides: fructose, saccharose, xylitol and glucose, where 16.5 mM of each saccharide was added to DMEM containing 5.5 mM of glucose to adjust the concentration (Fig. 2B). Hydrogen peroxide (0.1 mM) induced Hc cell death at a high concentration of glucose only, and not at high concentrations of the other saccharides.

Hc cell viability is rapidly decreased by hydrogen peroxide in a high glucose condition. The decline of Hc cell viability was detected after 15 min exposure to hydrogen peroxide (0.1 mM) in a high glucose culture condition (Fig. 3). Thereafter, cell viability rapidly decreased. Viable cells were rarely observed after 120 min exposure to hydrogen peroxide.

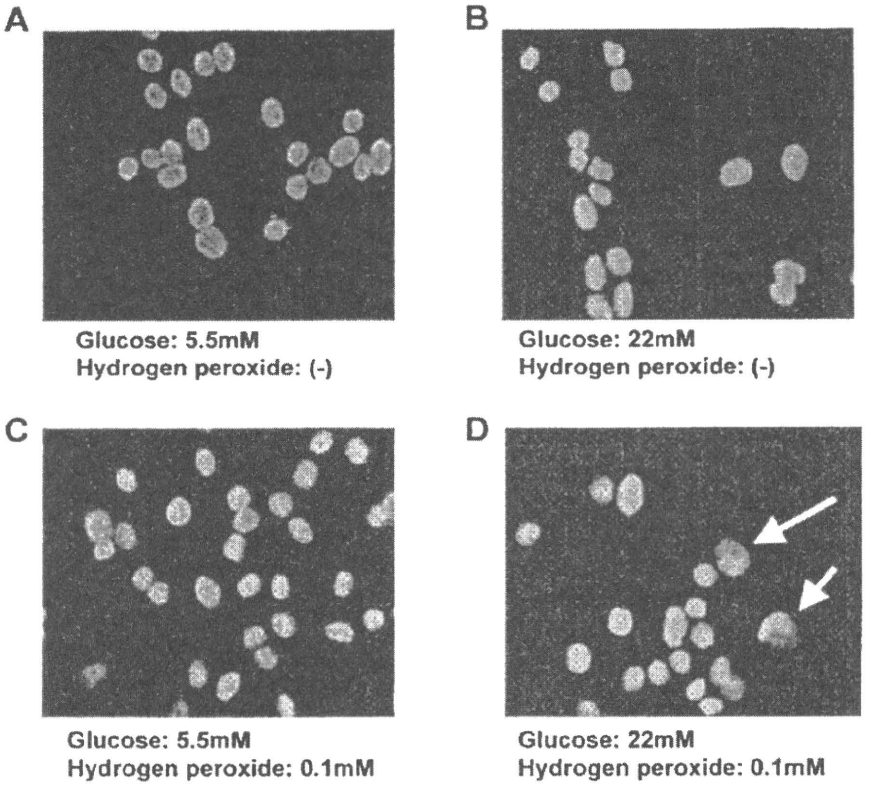

Figure 4. Hoechst staining of dying Hc cells. Hc cells were incubated for 120 min in 5.5 mM (A) and 22 mM (B) glucose without hydrogen peroxide, or 5.5 mM (C) or 22 mM (D) glucose with 0.1 mM hydrogen peroxide, then stained by Hoechst 33258 as described in Materials and methods. Representative data from four experiments are shown.

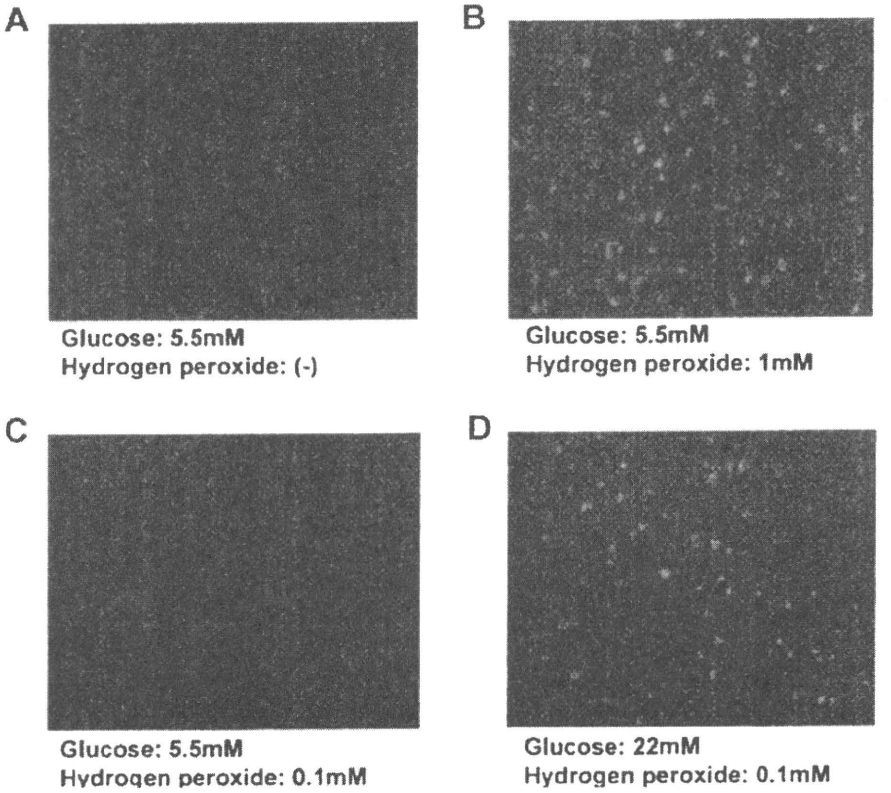

Figure 5. Sytox green staining of dying Hc cells. Hc cells were incubated for 120 min in 5.5 mM glucose without hydrogen peroxide (A), 5.5 mM glucose with 1 mM hydrogen peroxide (B), 5.5 mM glucose with 0.1 mM hydrogen peroxide (C) or 22 mM glucose with 0.1 mM hydrogen peroxide (D), then stained with Sytox green as described in Materials and methods. Representative data from four experiments are shown.

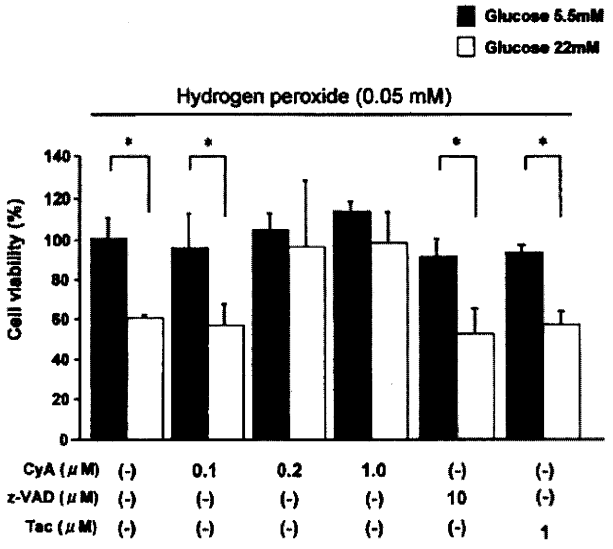

Figure 6. Effect of cyclosporine A (CyA), tacrolimus (Tac) or z-VAD on cell death induced by hydrogen peroxide under high glucose conditions. Hc cells were treated for 120 min with 0.05 mM hydrogen peroxide in medium containing 5.5 or 22 mM glucose. The indicated concentrations of CyA, Tac or z-VAD were added to the medium 30 min before treatment. Cell viability in each culture condition is expressed as a percentage compared to the viability of the control (5.5 mM glucose medium with 0.05 mM hydrogen peroxide). Data represent the mean ± SD values of four independent experiments. *p<0.01.

Hydrogen peroxide-treated Hc cells have enlarged and Sytox green-stained nuclei. To determine the mode of cell death, the nuclei of Hc cells were stained with Hoechst 33258 (Fig. 4) and Sytox green (Fig. 5) 2 h after hydrogen peroxide treatment. Hoechst 33258 staining indicated no structural changes in the nuclei of Hc cells in normal glucose, high glucose or normal glucose with hydrogen peroxide (0.1 mM) culture conditions (Fig. 4A, B and C). However, in high glucose culture conditions, Hc cells exposed to hydrogen peroxide (0.1 mM) showed expanded rather than condensed nuclei, indicating apoptosis (Fig. 4D). Hc cells were also stained with Sytox green, which penetrates cells with compromised plasma membranes but does not cross the membranes of apoptotic bodies. Sytox green-stained nuclei were detected in cells treated with 1 mM hydrogen peroxide in a normal glucose condition (Fig. 5B) or with 0.1 mM hydrogen peroxide in a high glucose condition (Fig. 5D), but not in the cells incubated in a normal glucose condition with or without 0.1 mM of hydrogen peroxide (Fig. 5A and C).

Cyclosporine A, but not z-VAD or tacrolimus, rescues Hc cells from hydrogen peroxide-induced cell death. We finally examined whether CyA or z-VAD restores Hc cell death induced by 0.05 mM of hydrogen peroxide in a high glucose condition. CyA, an inhibitor of calcineurin, has a property which inhibits mitochondrial permeability transition (MPT) pores, resulting in the inhibition of necrotic cell death (33). z-VAD, a pan-caspase inhibitor, blocks caspase-dependent cell death such as apoptosis. Pre-incubation with 0.2 and 1.0 μM of CyA 30 min before exposure to 0.05 mM hydrogen peroxide in a high glucose condition recovered cell viability to the level observed in 0.05 mM hydrogen peroxide in a normal glucose concentration, but z-VAD did not (Fig. 6). Tac, another calcineurin inhibitor that does not affect MPT activity, showed no effect on cell viability.

Discussion

Several mechanisms of cell death in response to hydrogen oxide have been proposed (34-38). Of these, Peiro *et al* reported that a high concentration of hydrogen oxide induces necrosis and a low one apoptosis in human aortic smooth muscle cells (38). Han *et al* showed that sub-lethal levels of hydrogen oxide sensitized cultured hepatocytes to TNF-induced apoptosis. High levels of hydrogen oxide triggered necrosis in hepatocytes regardless of whether TNF was present (34). In the present study, 0.05-0.1 mM of hydrogen peroxide did not have the ability to kill Hc cells under normal glucose culture conditions. However, in a high glucose culture condition, they effectively induced Hc cell death. This cell death was characterized by rapid induction, the expansion of nuclei (39), weakness of the nuclear membrane (40), no condensation of nuclei and no restoration of cell death by a pan-caspase inhibitor. These results suggest that the mode of cell death observed in this study could be necrosis rather than apoptosis (41). In addition to the above findings, the synergic effect of high glucose and hydrogen peroxide on cell death was blocked by CyA. Since CyA inhibits MPT pores, it is possible that the mechanism of cell death was MPT dependent. CyA also inhibited Hc cell death induced by a high concentration of hydrogen peroxide (1 mM) (data not shown). A similar observation was reported regarding high glucose-induced endothelial cell death.through a MPT-dependent process, which was prevented in the presence of CyA (42). These findings suggest a synergistic mechanism where high glucose induces the inhibition of MPT activity, while the addition of low-dose hydrogen peroxide leads to MPT-related cell death. A high glucose condition might elevate the sensitivity of hepatocytes to ROS, including hydrogen peroxide. This is consistent with the observation reported by Bouvard *et al* that HeLa-tat cells, which are stably transfected with the tat gene from human immunodeficiency virus type 1 and have a decreased antioxidant potential, exhibit necrosis or apoptosis under high glucose (20 mM) culture conditions, while parental HeLa cells do not (42).

The relationship between CyA and cell death was recently clarified. Necrosis involves the opening of pores in the inner mitochondrial membrane, known as MPT pores (44). This process is triggered by the accumulation of calcium inside the mitochondria and an increase in oxygen-free radicals that accompanies reperfusion (45). MPT pores have three components, adenine nucleotide translocase, voltage-dependent anion transporter and cyclophilin D (CypD). CyA binds to CypD, preventing it from binding to the adenine nucleotide translocase and strongly inhibiting MPT activity (46),which leads to ATP depletion and necrotic cell death (47). MPT is a key in necrotic cell death caused by oxidative stress, but is rarely involved in apoptosis. The mechanism by which CyA inhibits MPT has been attributed to its inhibitory effect on the peptidyl-prolyl isomerse activity of CypD, believed to be required for the formation of the MPT complex and MPT activation (46).

The coexistence of high glucose and hydrogen peroxide is a situation of clinical importance. A previous report (24) revealed that the association of elevated liver enzymes and postprandial hyperglycemia is adequate for the early diagnosis of NASH (48). Additionally, it was reported that acarbose (49), an α-glucosidase inhibitor, improves postprandial hyperglycemia by delaying the absorption of glucose. In addition, a ß-cell stimulator improves postprandial hyperglycemia by early stimulation of insulin and attenuates NASH. It is possible that hepatocytes escape cell death due to the improvement of postprandial hyperglycemia provided by these drugs. However, the influence of glucose concentrations on liver disease has not been thoroughly investigated. CyA, a useful immunosuppressant, might be suitable for immunosuppression following liver transplantation. This is because transplanted patients are susceptible to diabetes (50), and liver grafts are exposed to oxidative stress such as ischemic-reperfusion stress (51), suggesting that the damaged grafted liver, along with hyperglycemia, increases the risk of hepatocyte death.

This study demonstrated that the combination of high glucose and hydrogen peroxide causes necrotic hepatocyte death. This necrotic cell death is thought to be a MPT-related cell death because it is blocked by CyA. Clinically, hyperglycemia, a factor of metabolic syndrome, is often associated with ROS in the liver. Therefore, it is necessary to examine the influence of glucose concentrations on patients with HCV infection, NASH and ALD and who are undergoing liver transplantation.

References

1. Mates JM: Effects of antioxidant enzymes in the molecular control of reactive oxygen species toxicology. Toxicology 153: 83-104, 2000.
2. Jaeschke H: Preservation injury: mechanisms, prevention and consequences. J Hepatol 25: 774-780, 1996.
3. Forman HJ and Torres M: Reactive oxygen species and cell signaling: respiratory burst in macrophage signaling. Am J Respir Crit Care Med 166: S4-S8, 2002.
4. Bailey SM and Cunningham CC: Acute and chronic ethanol increases reactive oxygen species generation and decreases viability in fresh, isolated rat hepatocytes. Hepatology 28: 1318-1326, 1998.
5. Garcia-Ruiz C and Fernandez-Checa JC: Mitochondrial glutathione: hepatocellular survival-death switch. J Gastroenterol Hepatol 21 (Suppl 3): 3-6, 2006.
6. Lonardo A, Adinolfi LE, Loria P, Carulli N, Ruggiero G and Day CP: Steatosis and hepatitis C virus: mechanisms and significance for hepatic and extrahepatic disease. Gastroenterology 126: 586-597, 2004.
7. Mehta K, van Thiel DH, Shah N and Mobarhan S: Non-alcoholic fatty liver disease: pathogenesis and the role of antioxidants. Nutr Rev 60: 289-293, 2002.
8. Korenaga M, Wang T, Li Y, Showalter LA, Chan T, Sun J and Weinman SA: Hepatitis C virus core protein inhibits mitochondrial electron transport and increases reactive oxygen species (ROS) production. J Biol Chem 280: 37481-37488, 2005.
9. Okuda M, Li K, Beard MR, Showalter LA, Scholle F, Lemon SM and Weinman SA: Mitochondrial injury, oxidative stress, and antioxidant gene expression are induced by hepatitis C virus core protein. Gastroenterology 122: 366-375, 2002.
10. Valgimigli M, Valgimigli L, Trere D, Gaiani S, Pedulli GF, Gramantieri L and Bolondi L: Oxidative stress EPR measurement in human liver by radical-probe technique. Correlation with etiology, histology and cell proliferation. Free Radic Res 36: 939-948, 2002.
11. Alonzi T, Agrati C, Costabile B, Cicchini C, Amicone L, Cavallari C, Rocca CD, Folgori A, Fipaldini C, Poccia F, Monica NL and Tripodi M: Steatosis and intrahepatic lymphocyte recruitment in hepatitis C virus transgenic mice. J Gen Virol 85: 1509-1520, 2004.
12. Koike K, Moriya K and Kimura S: Role of hepatitis C virus in the development of hepatocellular carcinoma: transgenic approach to viral hepatocarcinogenesis. J Gastroenterol Hepatol 17: 394-400, 2002.
13. Sanchez A, Factor VM, Espinoza LA, Schroeder IS and Thorgeirsson SS: *In vitro* differentiation of rat liver derived stem cells results in sensitization to TNFalpha-mediated apoptosis. Hepatology 40: 590-599, 2004.
14. Ito Y, Oumi S, Nagasawa T and Nishizawa N: Oxidative stress induces phosphoenolpyruvate carboxykinase expression in H4IIE cells. Biosci Biotechnol Biochem 70: 2191-2198, 2006.
15. Khamaisi M, Kavel O, Rosenstock M, Porat M, Yuli M, Kaiser N and Rudich A: Effect of inhibition of glutathione synthesis on insulin action: *in vivo* and *in vitro* studies using buthionine sulfoximine. Biochem J 349: 579-586, 2000.
16. Schattenberg JM, Wang Y, Singh R, Rigoli RM and Czaja MJ: Hepatocyte CYP2E1 overexpression and steatohepatitis lead to impaired hepatic insulin signaling. J Biol Chem 280: 9887-9894, 2005.
17. Viberti G: Thiazolidinediones-benefits on microvascular complications of type 2 diabetes. J Diabetes Complications 19: 168-177, 2005.
18. Vanhorebeek I, De Vos R, Mesotten D, Wouters PJ, De Wolf-Peeters C and van den Berghe G: Protection of hepatocyte mitochondrial ultrastructure and function by strict blood glucose control with insulin in critically ill patients. Lancet 365: 53-59, 2005.
19. Lorenzi M, Cagliero E and Toledo S: Glucose toxicity for human endothelial cells in culture. Delayed replication, disturbed cell cycle, and accelerated death. Diabetes 34: 621-627, 1985.
20. Cai L, Li W, Wang G, Guo L, Jiang Y and Kang YJ: Hyperglycemia-induced apoptosis in mouse myocardium: mitochondrial cytochrome C-mediated caspase-3 activation pathway. Diabetes 51: 1938-1948, 2002.
21. Vincent AM, Stevens MJ, Backus C, McLean LL and Feldman EL: Cell culture modeling to test therapies against hyperglycemia-mediated oxidative stress and injury. Antioxid Redox Signal 7: 1494-1506, 2005.
22. Fiordaliso F, Leri A, Cesselli D, Limana F, Safai B, Nadal-Ginard B, Anversa P and Kajstura J: Hyperglycemia activates p53 and p53-regulated genes leading to myocyte cell death. Diabetes 50: 2363-2375, 2001.
23. Susztak K, Raff AC, Schiffer M and Bottinger EP: Glucose-induced reactive oxygen species cause apoptosis of podocytes and podocyte depletion at the onset of diabetic nephropathy. Diabetes 55: 225-233, 2006.
24. Paradis V, Perlemuter G, Bonvoust F, Dargere D, Parfait B, Vidaud M, Conti M, Huet S, Ba N, Buffet C and Bedossa P: High glucose and hyperinsulinemia stimulate connective tissue growth factor expression: a potential mechanism involved in progression to fibrosis in nonalcoholic steatohepatitis. Hepatology 34: 738-744, 2001.
25. Sugimoto R, Enjoji M, Kohjima M, Tsuruta S, Fukushima M, Iwao M, Sonta T, Kotoh K, Inoguchi T and Nakamuta M: High glucose stimulates hepatic stellate cells to proliferate and to produce collagen through free radical production and activation of mitogen-activated protein kinase. Liver Int 25: 1018-1026, 2005.
26. Wanless IR and Shiota K: The pathogenesis of nonalcoholic steatohepatitis and other fatty liver diseases: a four-step model including the role of lipid release and hepatic venular obstruction in the progression to cirrhosis. Semin Liver Dis 24: 99-106, 2004.
27. Powell EE, Jonsson JR and Clouston AD: Steatosis: co-factor in other liver diseases. Hepatology 42: 5-13, 2005.
28. Browning JD and Horton JD: Molecular mediators of hepatic steatosis and liver injury. J Clin Invest 114: 147-152, 2004.
29. Raval J, Lyman S, Nitta T, Mohuczy D, Lemasters JJ, Kim JS and Behrns KE: Basal reactive oxygen species determine the susceptibility to apoptosis in cirrhotic hepatocytes. Free Radic Biol Med 41: 1645-1654, 2006.
30. Chen L, Kwong M, Lu R, Ginzinger D, Lee C, Leung L and Chan JY: Nrf1 is critical for redox balance and survival of liver cells during development. Mol Cell Biol 23: 4673-4686, 2003.
31. Bedogni G, Miglioli L, Masutti F, Tiribelli C, Marchesini G and Bellentani S: Prevalence of and risk factors for nonalcoholic fatty liver disease: the Dionysos nutrition and liver study. Hepatology 42: 44-52, 2005.
32. Adams LA, Angulo P, Abraham SC, Torgerson H and Brandhagen D: The effect of the metabolic syndrome, hepatic steatosis and steatohepatitis on liver fibrosis in hereditary hemochromatosis. Liver Int 26: 298-304, 2006.

33. Lemasters JJ, Nieminen AL, Qian T, Trost LC, Elmore SP, Nishimura Y, Crowe RA, Cascio WE, Bradham CA, Brenner DA and Herman B: The mitochondrial permeability transition in cell death: a common mechanism in necrosis, apoptosis and autophagy. Biochim Biophys Acta 1366: 177-196, 1998.
34. Han D, Hanawa N, Saberi B and Kaplowitz N: Hydrogen peroxide and redox modulation sensitize primary mouse hepatocytes to TNF-induced apoptosis. Free Radic Biol Med 41: 627-639, 2006.
35. Gechev TS and Hille J: Hydrogen peroxide as a signal controlling plant programmed cell death. J Cell Biol 168: 17-20, 2005.
36. Daroui P, Desai SD, Li TK, Liu AA and Liu LF: Hydrogen peroxide induces topoisomerase I-mediated DNA damage and cell death. J Biol Chem 279: 14587-14594, 2004.
37. Ren D, Yang H and Zhang S: Cell death mediated by MAPK is associated with hydrogen peroxide production in Arabidopsis. J Biol Chem 277: 559-565, 2002.
38. Peiro C, Lafuente N, Matesanz N, Cercas E, Llergo JL, Vallejo S, Rodriguez-Manas L and Sanchez-Ferrer CF: High glucose induces cell death of cultured human aortic smooth muscle cells through the formation of hydrogen peroxide. Br J Pharmacol 133: 967-974, 2001.
39. Pozarowski P, Halicka DH and Darzynkiewicz Z: NF-kappaB inhibitor sesquiterpene parthenolide induces concurrently atypical apoptosis and cell necrosis: difficulties in identification of dead cells in such cultures. Cytometry A 54: 118-124, 2003.
40. Conde de la Rosa L, Schoemaker MH, Vrenken TE, Buist-Homan M, Havinga R, Jansen PL and Moshage H: Superoxide anions and hydrogen peroxide induce hepatocyte death by different mechanisms: involvement of JNK and ERK MAP kinases. J Hepatol 44: 918-929, 2006.
41. Simm A, Bertsch G, Frank H, Zimmermann U and Hoppe J: Cell death of AKR-2B fibroblasts after serum removal: a process between apoptosis and necrosis. J Cell Sci 110: 819-828, 1997.
42. Bouvard S, Faure P, Roucard C, Favier A and Halimi S: Characterization of free radical defense system in high glucose cultured HeLa-tat cells: consequences for glucose-induced cytotoxicity. Free Radic Res 36: 1017-1022, 2002.
43. Detaille D, Guigas B, Chauvin C, Batandier C, Fontaine E, Wiernsperger N and Leverve X: Metformin prevents high-glucose-induced endothelial cell death through a mitochondrial permeability transition-dependent process. Diabetes 54: 2179-2187, 2005.
44. Vande Velde C, Cizeau J, Dubik D, Alimonti J, Brown T, Israels S, Hakem R and Greenberg AH: BNIP3 and genetic control of necrosis-like cell death through the mitochondrial permeability transition pore. Mol Cell Biol 20: 5454-5468, 2000.
45. Halestrap AP: Calcium, mitochondria and reperfusion injury: a pore way to die. Biochem Soc Trans 34: 232-237, 2006.
46. Nakagawa T, Shimizu S, Watanabe T, Yamaguchi O, Otsu K, Yamagata H, Inohara H, Kubo T and Tsujimoto Y: Cyclophilin D-dependent mitochondrial permeability transition regulates some necrotic but not apoptotic cell death. Nature 434: 652-658, 2005.
47. Kim JS, He L and Lemasters JJ: Mitochondrial permeability transition: a common pathway to necrosis and apoptosis. Biochem Biophys Res Commun 304: 463-470, 2003.
48. Gholam PM, Flancbaum L, Machan JT, Charney DA and Kotler DP: Nonalcoholic fatty liver disease in severely obese subjects. Am J Gastroenterol 102: 399-408, 2007.
49. Lieber CS, Leo MA, Mak KM, Xu Y, Cao Q, Ren C, Ponomarenko A and De Carli LM: Acarbose attenuates experimental non-alcoholic steatohepatitis. Biochem Biophys Res Commun 315: 699-703, 2004.
50. John PR and Thuluvath PJ: Outcome of patients with new-onset diabetes mellitus after liver transplantation compared with those without diabetes mellitus. Liver Transpl 8: 708-713, 2002.
51. Burke A, FitzGerald GA and Lucey MR: A prospective analysis of oxidative stress and liver transplantation. Transplantation 74: 217-221, 2002.

Tum-1, a tumstatin fragment, gene delivery into hepatocellular carcinoma suppresses tumor growth through inhibiting angiogenesis

TAKASHI GOTO[1], HIROKI ISHIKAWA[1], KOJIRO MATSUMOTO[1], DAISUKE NISHIMURA[1], MARIKO KUSABA[1], NAOTA TAURA[1], HIDETAKA SHIBATA[1], HISAMITSU MIYAAKI[1] TATSUKI ICHIKAWA[1], KEISUKE HAMASAKI[1], KAZUHIKO NAKAO[1], YOHEI MAESHIMA[2] and KATSUMI EGUCHI[1]

[1]First Department of Internal Medicine, Nagasaki University School of Medicine, 1-7-1 Sakamoto, Nagasaki 852-8501; [2]Department of Medicine and Clinical Science, Okayama University Graduate School of Medicine, Dentistry and Pharmaceutical Sciences, Okayama, Japan

Received December 27, 2007; Accepted February 5, 2008

Abstract. Since hepatocellular carcinoma (HCC) is a hypervascular cancer, anti-angiogenic therapy is a promising approach to treat HCC. In the present study, we investigated the antiangiogenic and antitumor effects of tum-1, a fragment of tumstatin, gene transduction into HCC *in vitro* and *in vivo*. Tum-1 gene was cloned into a pSecTag2B mammalian expression vehicle to construct pSecTag2B-tum-1. pSecTag2B-tum-1 or vehicle were transfected into human HCC cells, PLC/PRF/5 cells stably and Huh-7 cells transiently. pSecTag2B-tum-1 transfection slightly repressed the proliferation of both PLC/PRF/5 and Huh-7 cells *in vitro*. Addition of conditioned media (CM) from tum-1 expressing PLC/PRF/5 cells significantly inhibited the spontaneous and vascular endothelial growth factor (VEGF)-induced proliferation and migration of human umbilical vein endothelial cells (HUVEC) *in vitro* with diminishing the VEGF-induced phosphorylation of both Akt and extracellular signal-regulated kinase (ERK) that are known to mediate VEGF-induced proliferation and migration of endothelial cells. In *in vivo* experiments, intratumoral injection of pSecTag2B-tum-1 significantly repressed the growth of pre-established Huh-7 tumors in athymic mouse models accompanying the decreased density of CD34 positive vessels in tumors. In conclusion, our results suggest that antiangiogenic gene therapy using tum-1 gene may be an efficient strategy for the treatment of HCC.

Correspondence to: Dr Kazuhiko Nakao, First Department of Internal Medicine, Nagasaki University School of Medicine, 1-7-1 Sakamoto, Nagasaki 852-8501, Japan
E-mail: kazuhiko@net.nagasaki-u.ac.jp

Key words: tum-1, tumstatin, hepatocellular carcinoma, angiogenesis

Introduction

Hepatocellular carcinoma (HCC) is one of the most common fatal malignancies worldwide, and is especially common in several parts of Asia and Africa (1). Although advances in medical technology have permitted the early recognition and treatment of HCC (1,2), the annual death rate from HCC exceeds 30,000 in Japan (3). Therefore, there is a need to develop new strategies to treat HCC.

Recently, it has been reported that antiangiogenic agents sufficiently inhibit tumor growth *in vivo* (4). Since HCC is a hypervascular cancer, antiangiogenic therapy might be particularly effective in the treatment of patients with HCC. However, systemic administration of antiangiogenic agents, such as thalidomide (5) or TNP-470 (6), might not be the most efficient method for locally aggressive tumors. Therefore, it is conceivable that antiangiogenic gene delivery to cancer cells could be suitable for the treatment of HCC, where it can increase the local concentration of therapeutic endogenous agents. In fact, we have reported that the introduction of antiangiogenic genes such as angiostatin and pigment epithelium-derived factor (PEDF) genes into HCC cells exhibited significant antitumor effect in xenograft models (7,8).

The noncollagenous domain of α3 chain of type IV collagen, namely tumstatin, has the antiangiogenic property by inhibiting endothelial cell proliferation and inducing their apoptosis via an interaction with αvß3 integrin (9-15). Antiangiogenic effect of tumstatin has been studied in xenograft models, where tumstatin repressed the growth of several cancer types including renal cell carcinoma, prostate cancer, melanoma and lung carcinoma (9-11,13). In the present study, we constructed a mammalian expression vector expressing tum-1 which consists of 54-244 amino acids of tumstatin and has antiangiogenic activity (9). Following stable transfection of this vector into HCC cells, we examined the antiangiogenic activity of tum-1 using cultured human umbilical vein endothelial cells (HUVEC) in the presence or

absence of vascular endothelial growth factor (VEGF). In addition, we investigated the antiangiogenic and antitumor effects of tum-1 *in vivo* by intratumoral injection of tum-1 expression vector into HCC tumor implanted subcutaneously in athymic nude mice.

Materials and methods

Cell culture. Human HCC cell lines, PLC/PRF/5 and Huh-7 cells, were maintained in RPMI supplemented with 10% bovine calf serum. Human umbilical vascular endothelial cells (HUVEC) were purchased from Sankyo Junyaku (Tokyo, Japan) and were grown in endothelial cell growth medium 2. HUVEC were grown to <6 passages for all experiments.

Plasmid construction and transfection. The human tum-1 cDNA was kindly provided by Dr Y. Maeshima (Department of Medicine and Clinical Science, Okayama University, Japan) and cloned into pSecTag2B mammalian expression vector containing hexahistidine tag (Invitrogen, Carlsbad, CA) to construct pSecTag2B-tum-1. To establish the PLC/PRF/5 cells stably expressing tum-1/hexahistidine chimera protein, 10 μg of pSecTag2B-tum-1 was transfected into the cells by the lipofection method (Life Technologies, Inc., Gaithersburg, MD). After transfection, the cells were cultured in fresh medium containing Zeocin (100 μg/ml) for 2 weeks. Zeocin-resistant pooled populations were subjected to further studies. As a control, pSecTag2B vehicle was also stably transfected into PLC/PRF/5 cells. In addition, pSecTag2B vehicle or pSecTag2B-tum-1 was transiently transfected into Huh-7 cells.

Preparation of conditioned media. PLC/PRF/5 cells stably transfected with pSecTag2B-tum-1 or vehicle were plated on 100-mm dishes. After 24 h, the medium was replaced with 5 ml serum-free RPMI and incubated for 48 h. Then, conditioned media (CM) from pSecTag2B-tum-1-transfected PLC/PRF/5 cells (CM-tum-1), vehicle-transfected PLC/PRF/5 cells (CM-Mock) and non-transfected PLC/PRF/5 cells (CM-N) were collected and used in the assay. In some experiments, CM-tum-1 was passed through the His trap kit (Amersham Life Science, Buckinghamshire, UK) and the flow-through fraction (CM-tum-1ΔHis) was collected and used in the assay. Similarly, CM from Huh-7 cells transiently transfected with SecTag2B-tum-1 (CM-tum-1) and vehicle (CM-Mock) or CM from non-transfected Huh-7 cells (CM-N) were collected and used in the assay.

Proliferation of hepatoma cells. PLC/PRF/5 cells stably transfected with vehicle (Mock) or pSecTag2B-tum-1 (tum-1) were seeded onto 96-well culture plates at ~5x10^3 cells/well and were incubated for 72 h. Cell proliferation was evaluated using the CellTiter 96 Aqueous One Solution Cell Proliferation Assay kit (Promega, Madison, WI). Similarly, non-transfected PLC/PRF/5 cells were seeded onto 96-well culture plates. After 24 h, the medium was replaced with 100 μl of CM-N, CM-Mock, CM-tum-1 and CM-tum-1ΔHis. After 48 h, cell proliferation was determined. Whereas, Huh-7 cells seeded onto 96-well culture plates were transiently transfected with vehicle (Mock) or pSecTag2B-tum-1 (tum-1) and cultured for 48 h, and cell proliferation was determined.

Proliferation and migration of HUVEC. HUVECs were plated onto 96-well culture plates at approximately 5x10^3 cells/well and incubated for 24 h. Medium was replaced with 100 μl of CM-Mock or CM-tum-1 with or without 10 ng/ml of recombinant human vascular endothelial growth factor (VEGF, R&D systems, Minneapolis, MN, USA). After 48 h, cell proliferation was determined by the CellTiter 96 Aqueous One Solution Cell Proliferation Assay kit. Migration of HUVEC was analyzed using 8.0-μm 24-well Transwells (Corning, Acton, MA) as described previously (7,8). Briefly, 600 μl of CM-Mock or CM-tum-1 with or without 10 ng/ml of VEGF was placed in the lower chamber. HUVEC (~2x10^4) suspended in 200 μl of serum-free RPMI were added to the upper chamber. After 24-h incubation, non-migrating cells were removed from the upper surface of the membrane with a cotton swab. Cells migrating to the lower surface were fixed with methanol and stained with Giemsa. Cell number was counted with a light microscope under a high power field (magnification x200).

Western blotting. HUVEC were incubated with CM-Mock or CM-tum-1 in the presence or absence of 10 ng/ml of VEGF for 30 min. Then, the cells were washed twice with phosphate-buffered saline (PBS), lysed by addition of lysis buffer [50 mM Tris (pH 8.0), 150 mM NaCl, 0.02% sodium azide, 0.1% SDS, 100 μg/ml PMSF, 1 μg/ml of aprotinin, 1% NP40, 0.5% sodium deoxycholate and 1 mM sodium o-vanadate] for 10 min at 4°C, and insoluble materials were removed by centrifugation at 14,000 rpm for 30 min at 4°C. The supernatant was collected, and the protein concentration was determined using a Bio-Rad protein assay kit (Melville, NY, USA). The same amount of protein from each lysate or conditioned medium (10 μg/well) was analyzed by electrophoresis on 8-12% SDS polyacrylamide gel and transblotted onto nitrocellulose membrane. Blots were blocked with a solution of 5% non-fat dry milk/Tris-buffered saline containing 0.1% Tween-20 (TBS-T) for 1 h and then incubated overnight at 4°C in the presence of rabbit anti-hexahistidine (ICN, Costa Mesa, CA), rabbit anti-human phosphor-Akt, rabbit anti-human Akt, rabbit anti-human phosphor-ERK1/2 and rabbit anti-human ERK1/2 (Cell Signaling, Beverly, MA, USA). The membranes were washed with TBS-T and were incubated with horseradish peroxidase-conjugated anti-rabbit immunoglobulin G. After washing with TBS-T, immunoreactive bands were visualized using the ECL chemiluminescence system (Amersham).

In vivo study. Four-week-old male BALB/c nu/nu athymic mice were purchased from Charles River (Yokohama, Japan). Animal experiments were performed in accordance with institutional guidelines, and the study was approved by the Ethics Committee of Nagasaki University. Huh-7 cells (3x10^6) were implanted subcutaneously into the left thigh. Tumor volume was calculated as follows; tumor volume = length (mm) x width^2 (mm) x 1/2. When the tumor volume reached 100 mm^3, pSecTag2B-tum-1 [75 μg plasmid/100 μl of TE (Tris ethylenediamine tetra acetic acid) buffer] with 20 μl of lipofectin was injected into the tumor at day 1, 8, 15 and 22. As a control, pSecTag2B vehicle (75 μg plasmid/100 μl of TE) with lipofectin was injected similarly. Each group consisted

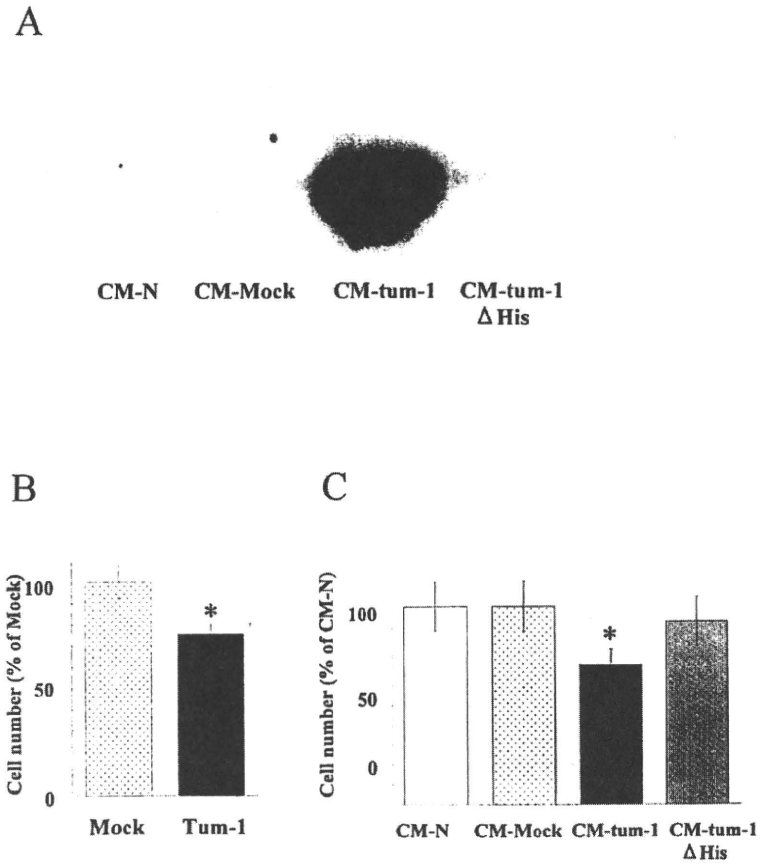

Figure 1. Growth of PLC/PRF/5 cells stably transfected with pSecTag2B-tum-1. (A) Expression of tum-1/hexahistidine chimera protein in CM from PLC/PRF/5 cells stably transfected with pSecTag2B-tum-1 was analyzed by Western blotting; CM-N, CM from non-transfected cells; CM-Mock, CM from vehicle transfected cells; CM-tum-1, CM from pSecTag2B-tum-1 transfected cells; CM-tum-1ΔHis, CM-tum-1 passed through His trap kit. (B) PLC/PRF/5 cells stably transfected with vehicle (Mock) or pSecTag2B-tum-1 (Tum-1) were cultured for 72 h, after which cell number was counted. Results are expressed as a percentage of Mock. Data represent the mean ± SD values of four separate experiments; *p<0.01 vs Mock. (C) CM shown in (A) was added to non-transfected PLC/PRF/5 cells, and cells were cultured for 48 h, then cell number was counted. Results are expressed as a percentage of CM-N. Data represent the mean ± SD values of four separate experiments; *p<0.01 vs CM-N, CM-Mock and CM-tum-1ΔHis.

of five mice. Tumor volume was measured every 2-3 days until 25 days after first injection. Tumors were removed and analyzed by reverse-transcriptase polymerase chain reaction (RT-PCR) and immunohistochemistry.

RT-PCR. Total RNA was extracted from tumors and PLC/PRF/5 cells stably transfected pSecTag2B-tum-1. RNA was used after contaminating DNA was completely removed by DNase I treatment. RT-PCR was performed according to the instructions provided by the supplier of the OneStep RT-PCR Kit (Qiagen, Valencia, CA), using primers specific for tum-1 derived from pSecTag2B-tum-1 and glyceraldehyde 3-phosphate dehydrogenase (GAPDH) as a control. Reaction mixtures (10 μl) were loaded on 1.2% agarose gels and visualized by ethidium bromide staining.

Immunohistochemistry. Immunohistochemistry was performed using anti-mouse CD34 antibody (Serotec Ltd., Oxford, UK) and anti-mouse αSMA (Actin, Smooth Muscle, Shandon Immunon™, USA). Tissue samples of the tumor extracted from each mouse were cut into 4-μm-thick sections and mounted on aminopropyltriethoxysilane-coated glass slides. Sections were immunostained with anti-CD34 at a dilution of 1:100 for 60 min using the Streptavidin Peroxidase technique (SAB) (Histomouse™ Plus Kits, Zymed Labolatories Inc., South San Francisco, USA). The second staining with anti-αSMA was conduced by making the section reactive primary antibody, anti-αSMA (dilution 1:100), at 4˚C overnight, and by using the SAB technique. The sections were stained with the mixture of a commercial chromogen (VIP) and hydrogen peroxide and hematoxylin for counterstaining.

Statistical analysis. All data were expressed as mean ± SD. Differences between groups were examined for statistical significance using Student's t-test. All reported p-values are two-tailed, and those <0.05 were considered statistically significant.

Results

Tum-1 gene introduction slightly represses the proliferation of HCC cells. Tum-1 expression plasmid (pSecTag2B-tum-1) was stably transfected into PLC/PRF/5 cells, and the secretion of tum-1 protein from the cells was analyzed by Western blotting. As shown in Fig. 1A, conditioned medium (CM) from PLC/PRF/5 cells stably transfected with pSecTag2B-

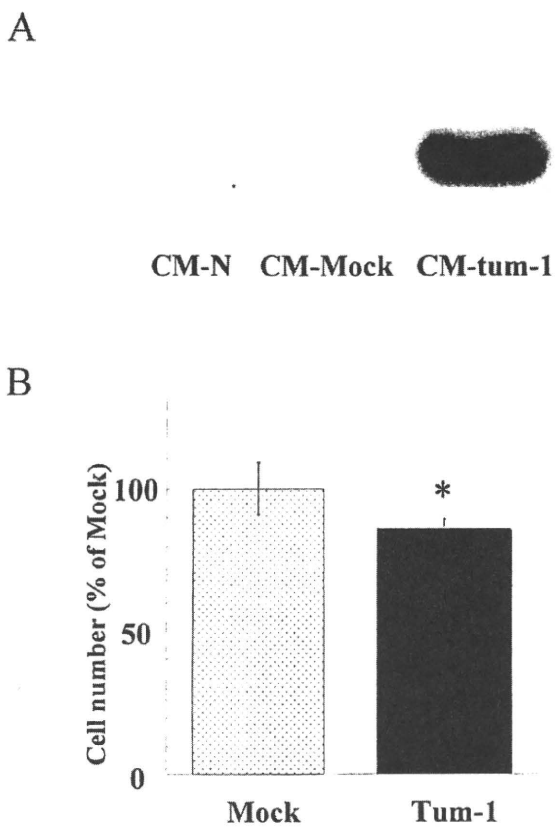

Figure 2. Growth of Huh-7 cells transiently transfected with pSecTag2B-tum-1. (A) Expression of tum-1/hexahistidine chimera protein in CM from Huh-7 cells transiently transfected with pSecTag2B-tum-1 was analyzed by Western blotting with using anti-His tag antibody, CM-N, CM from non-transfected cells; CM-Mock, CM from vehicle transfected cells; CM-tum-1, CM from pSecTag2B-tum-1 transfected cells. (B) Huh-7 cells transiently transfected with pSecTag2B-tum-1 (Tum-1) or vehicle (Mock) were incubated for 48 h, after which cell number was counted. Results are expressed as a percentage of Mock. Data represent the mean ± SD values of four separate experiments; *$p<0.05$ vs Mock.

tum-1 (CM-tum-1) contained the tum-1/hexahistidine chimera protein detected by anti-hexahistidine antibody, and this chimera protein was effectively removed by the His trap kit (CM-tum-1ΔHis) (Fig. 1A). Cell proliferation assay showed that the growth of PLC/PRF/5 cells stably transfected with pSecTag2B-tum-1 was slightly slower than that of PLC/PRF/5 cells stably transfected with vehicle (Mock) (Fig. 1B). To elucidate whether this growth suppression was mediated by tum-1/hexahistidine chimera protein, CM from PLC/PRF/5 cells stably transfected with pSecTag2B-tum-1 (CM-tum-1) was added to parental PLC/PRF/5 cells, which also retarded the growth of parental cells compared with addition of CM-tum-1 passed through His trap kit (CM-tum-1ΔHis) or CM from PLC/PRF/5 cells stably transfected with vehicle (CM-Mock) (Fig. 1C). Next, pSecTag2B-tum-1 was transiently transfected into Huh-7 cells, and effect on the cell growth was determined. As shown in Fig. 2A, CM from Huh-7 cells transiently transfected with pSecTag2B-tum-1 (CM-tum-1) contained the tum-1/hexahistidine chimera protein. The growth of Huh-7 was slightly repressed by transient transfection with pSecTag2B-tum-1 (Fig. 2B). These results suggest that tum-1 has a weak but significant antiproliferative activity against human HCC cells.

Tum-1 inhibits the spontaneous and VEGF-induced proliferation and migration of HUVEC. Next, we determined the effects of tum-1 on the spontaneous and VEGF-induced proliferation and migration of HUVEC. As shown in Fig. 3A, addition of CM from PLC/PRF/5 cells stably transfected with pSecTag2B-tum-1 (CM-tum-1) clearly inhibited both spontaneous and VEGF-induced proliferation of HUVEC compared with addition of CM from vehicle transfected cells (CM-Mock) (Fig. 3A). Similarly, addition of CM-tum-1 repressed the spontaneous and VEGF-induced migration of HUVEC (Fig. 3B). Since phosphatidylinositol 3-kinase (PI3K)-protein kinase B (PKB/Akt) and extracellular signal-regulated kinase (ERK) signaling pathways are involved in the VEGF-induced proliferation and migration of HUVEC (16-18), we analyzed the effects of tum-1 on the VEGF-induced phosphorylation of Akt and ERK by Western blotting (Fig. 4). Phosphorylation of both Akt and ERK was constitutively detected in HUVEC, which was further upregulated by VEGF. However, addition of CM-tum-1 repressed the VEGF-induced phosphorylation of both Akt and ERK to the basal level.

Antitumor effect of tum-1 gene introduction in vivo. Huh-7 cells were subcutaneously implanted and tumors were established in athymic nude mice because Huh-7 cells were more efficiently transplantable than other cell lines. After reaching an adequate size, the tumor was directly injected with pSecTag2B-tum-1, and the effect of treatment on tumor size was determined. Injection of pSecTag2B-tum-1 resulted in a significant reduction of tumor volume compared with vehicle-injected tumors at day 24 ($p<0.01$; Fig. 5). The expression of tum-1 mRNA in the pSecTag2B-tum-1-injected tumors (at day 24) was confirmed by RT-PCR (Fig. 6A), where the density of CD34 and αSMA positive vessels/fields was significantly lower than those in the vehicle-injected tumors (Fig. 6B and C). These results indicate that the tumor suppressive effect of tum-1 gene injection was closely related to the vascularity of tumors.

Discussion

Tumstatin, a non-collagenous domain of α3 chain of type IV collagen, consists of 244 amino acids (9,14), which is cleaved from type IV collagen by matrix metalloproteinase-9 (14,19). Tumstatin inhibits proliferation and causes apoptosis of endothelial cells through αvß3 integrin interaction in an RGD-independent manner (9-14). Tumstatin also inhibits tube formation of endothelial cells on Matrigel and induces G1 endothelial cell cycle arrest (14). Deletion mutants of tumstatin including tum-1 (54-244 amino acids), tum-2 (1-132 amino acids) and tum-5 (54-132 amino acids) retain the anti-angiogenic activity (9-11).

In the present study, tum-1 expression plasmid vector (pSecTag2B-tum-1) was introduced into HCC cells. HCC cells transfected with pSecTag2B-tum-1 produced the detectable tum-1/hexahistidine chimera protein in its CM. Surprisingly, stable and transient tum-1 gene transfection into PLC/PRF/5 and Huh-7 cells, respectively, slightly repressed

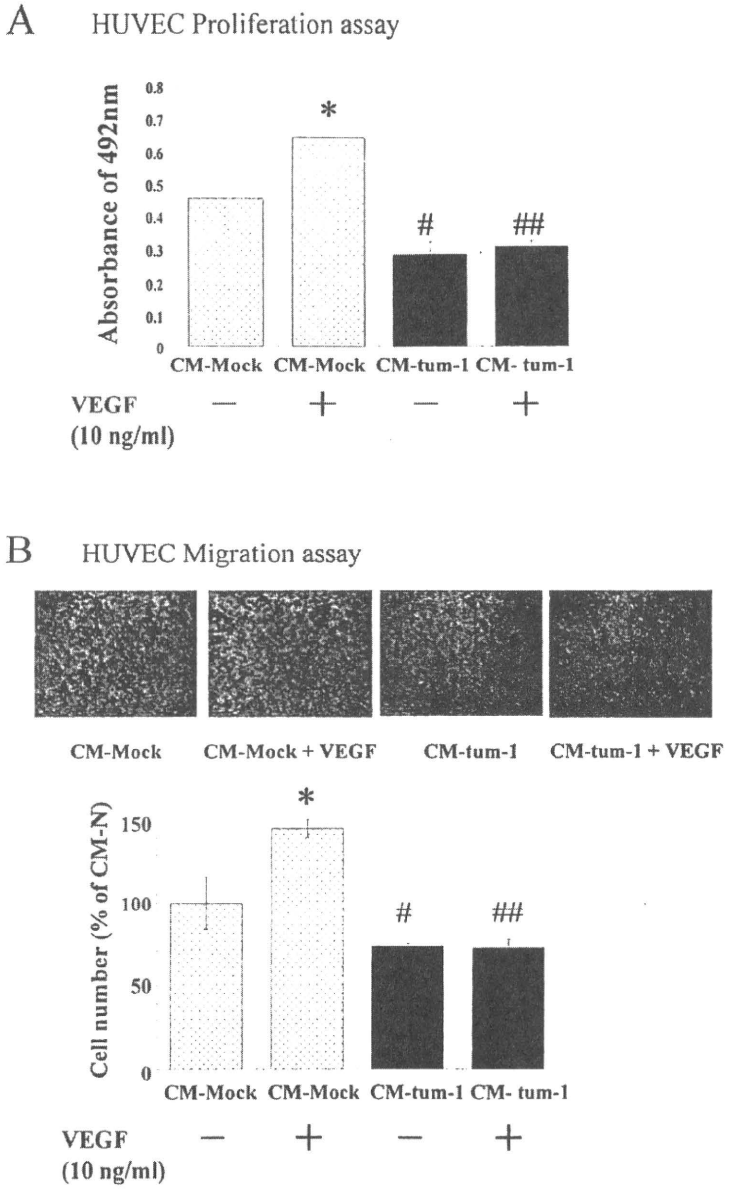

Figure 3. Effects of CM containing tum-1/hexahistidine chimera protein on proliferation and migration of HUVEC. (A) HUVEC were cultured on 96-well plates in 100 μl of CM derived from PLC/PRF/5 cells transfected with vehicle (CM-Mock) or pSecTag2B-tum-1 (CM-tum-1) in the presence or absence of VEGF (10 ng/ml). Cell number was determined after 48-h incubation. Results are expressed as a percentage of CM-Mock without VEGF. Data represent the mean ± SD values of four separate experiments; *p<0.01 vs CM-Mock without VEGF; #p<0.05 vs CM-Mock without VEGF; ##p<0.01 vs CM-Mock with VEGF. (B) CM-Mock or CM-tum-1 with or without VEGF was placed in the lower chamber of a modified Boyden chamber, and HUVEC were seeded to the upper chamber. After 24-h incubation, non-migrating cells were removed and cells that migrated through the membrane pores were stained with Giemsa and counted. Representative micrographs of migrated HUVEC in each CM are shown in upper panel. Results are expressed as a percentage of CM-Mock without VEGF. Data represent the mean ± SD values of four separate experiments; *p<0.01 vs CM-Mock without VEGF; #p<0.05 vs CM-Mock without VEGF; ##p<0.01 vs CM-Mock with VEGF.

the proliferation of these cells. Recent reports revealed that αvß3 integrin, the receptor of tumstatin, is expressed in several HCC cell lines including Huh-7 cells (20) and also in clinical samples of HCC (21). Therefore, it is possible that tum-1 could inhibit the proliferation of HCC cells through interacting with αvß3 integrin. Similar observation was reported that the gene introduction of tumstatin or its C-terminal residues 185-203 into melanoma cells directly inhibited the proliferation and invasiveness of these cells *in vitro* (22).

A potential mechanism of antiangiogenic function of tumstatin has been reported that tumstatin inhibits activation of focal adhesion kinase (FAK), phosphatidylinositol 3-kinase (PI3K), protein kinase B (PKB/Akt), and mammalian target of rapamycin (mTOR), and it prevents the dissociation of eukaryotic initiation factor 4E protein (eIF4E) from 4E-binding protein 1, resulted in the inhibition of cap-dependent protein synthesis in endothelial cells (23,24). Since PI3K-PKB/Akt signaling plays a key role in cell growth and survival in a variety of cells (25), it is conceivable that inhibition of this

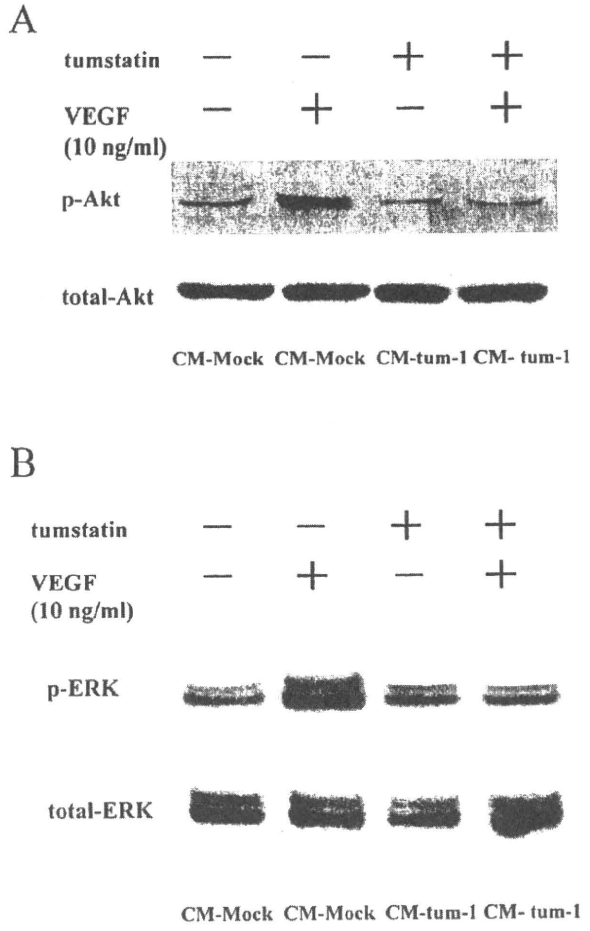

Figure 4. Effects of CM containing tum-1/hexahistidine chimera protein on spontaneous or VEGF-induced phosphorylation of Akt and ERK. Huh-7 cells were incubated with indicated CM with or without 10 ng/ml of VEGF for 30 min, and the levels of phosphorylation of Akt (A) or ERK (B) were analyzed by Western blotting. Results shown are from one representative experiment from a total of four performed.

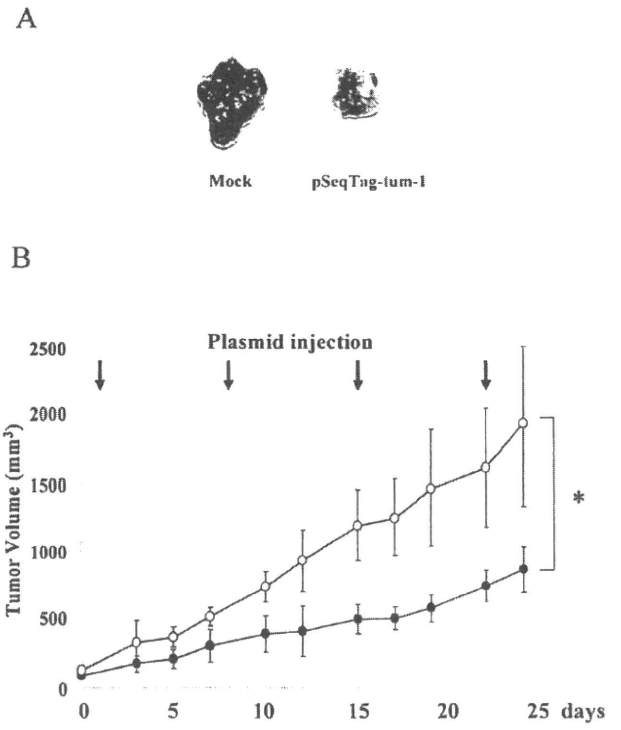

Figure 5. Inhibition of pre-established Huh-7 tumor growth by injection of pSecTag2B-tum-1 in athymic mice. Mock (vehicle; open circle) or pSecTag2B-tum-1 (closed circle) was injected intratumorally into pre-established tumors of Huh-7 cells. Mice were sacrificed on day 25, and subcutaneous tumors were extracted. (A) Representative photographs of harvested tumors. (B) Serial changes in tumor volume in the two groups. Data are mean ± SD (n=5); *p<0.01 vs vehicle.

signaling leads to the growth arrest and apoptosis of endothelial cells. Furthermore, recent studies revealed that VEGF promoted angiogenesis through activating PI3K-PKB/Akt signaling (16,17), and that luteolin, an antiangiogenic compound, repressed the VEGF-induced angiogenesis by inhibiting PI3K-PKB/Akt signaling (26). In contrast to tumstatin, endostatin, another antiangiogenic fragment released from α1 chain of type XVIII collagen, interacts with α5ß1 integrin and inhibits activation of FAK, and ras-raf-ERK signaling, but not PI3K-PKB/Akt signaling, and it prevents endothelial cell migration with no effect on proliferation and survival (24), indicating that tumstatin has a distinct antiangiogenic mechanism from endostatin. In this study, addition of CM containing tum-1 repressed not only spontaneous and VEGF-induced proliferation of HUVEC but also its migration, and clearly abolished the VEGF-induced phosphorylation of both Akt and ERK in HUVEC. This is surprising because tumstatin has been reported to inhibit, through binding to αvß3, the PI3K-PKB/Akt signaling and proliferation of endothelial cells rather than ras-raf-ERK signaling and migration of these cells (24). However, several studies have reported that αvß3 blocking antibody which has a similar antiangiogenic activity to tumsatain (27) inhibited the angiogenesis through blocking the ras-raf-ERK signaling (13), and that blocking of ras-raf-ERK signaling by PD98059 resulted in the inhibition of VEGF-induced proliferation of HUVEC (18). Taken together, it may be possible that there are several mechanisms mediating antiangiogenic function of tumstatin.

Non-viral gene delivery systems are less efficient at inducing transgene expression and have shorter-term expression compared with viral delivery systems. Despite the expected low efficiency of gene induction, intratumoral injection of tum-1 expression plasmid vector (pSecTag2B-tum-1) significantly repressed the Huh-7 tumor growth accompanying the decreased density of CD34 and αSMA positive vessels compared with vehicle injection. These results suggest that a sufficient bystander effect was achieved by this strategy, and if the transgene is expressed intratumorally, highly efficient therapeutic gene induction may not be necessarily required. We have reported that PEDF gene transduction into Huh-7 tumor significantly repressed its growth in athymic mouse models as well as tum-1 shown in this study, but PEDF did not directly inhibit the proliferation of Huh-7 cells *in vitro* (8). Therefore, it is likely that antitumor effect of tum-1 *in vivo* could be attributable to its anti-

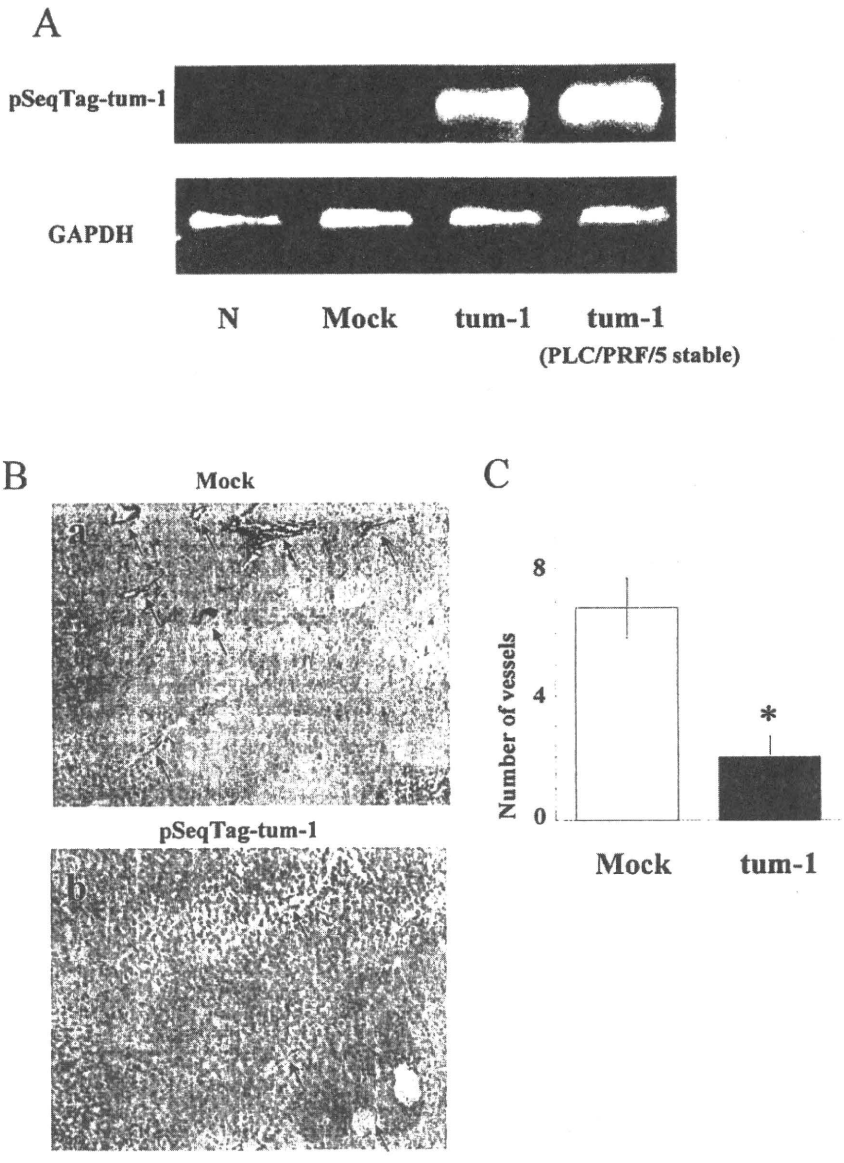

Figure 6. Tum-1 mRNA expression and CD34-positive vessel density in the tumors. (A) Exogenous tum-1 mRNA expression in the tumor was analyzed by RT-PCR. Total RNA was extracted from tumor tissues. RT-PCR was performed with primers specific for tum-1 and GAPDH (internal control). Total RNA from PLC/PRF/5 cells stably transfected with pSecTag2B-tum-1was used as a positive control (right column); N, negative control; Mock, vehicle injected tumor; tum-1, pSecTag2B-tum-1 injected tumor. (B) Representative photographs of a harvested tumor stained immunohistochemically with anti-CD34 and anti-αSMA antibody. Arrows indicate CD34 (brown) and αSMA (violet) positive vessels (original magnification x200); a, Mock (vehicle) injected tumor; b, pSecTag2B-tum-1 injected tumor. (C) Number of CD34 (brown) and αSMA (violet) positive vessels/field. Data represent a number of CD34 and αSMA positive vessels counted from the five different fields of each sample. Data are mean ± SD (n=5); *p<0.01 vs Mock.

angiogenic activity rather than direct antiproliferative activity against Huh-7 cells. In conclusion, it is possible that intratumoral gene injection of tumstatin or its active derivatives including tum-1 is a promising strategy for the treatment of HCC.

References

1. Llovet JM, Burroughs A and Bruix J: Hepatocellular carcinoma. Lancet 362: 1907-1917, 2003.
2. Sato Y, Nakata K, Kato Y, *et al*: Early recognition of hepatocellular carcinoma based on altered profiles of alpha-fetoprotein. N Engl J Med 328: 1802-1806, 1993.
3. Kiyosawa K and Tanaka E: Characteristics of hepatocellular carcinoma in Japan. Oncology 62 (Suppl. 1): 5-7, 2002.
4. Gaya AM and Rustin GJ: Vascular disrupting agents: a new class of drug in cancer therapy. Clin Oncol (R Coll Radiol) 17: 277-290, 2005.
5. Patt YZ, Hassan MM, Lozano RD, Ellis LM, Peterson JA and Waugh KA: Durable clinical response of refractory hepatocellular carcinoma to orally administered thalidomide. Am J Clin Oncol 23: 319-321, 2000.
6. Kin M, Torimura T, Ueno T, *et al*: Angiogenesis inhibitor TNP-470 suppresses the progression of experimentally-induced hepatocellular carcinoma in rats. Int J Oncol 16: 375-382, 2000.
7. Ishikawa H, Nakao K, Matsumoto K, *et al*: Antiangiogenic gene therapy for hepatocellular carcinoma using angiostatin gene. Hepatology 37: 696-704, 2003.

8. Matsumoto K, Ishikawa H, Nishimura D, Hamasaki K, Nakao K and Eguchi K: Antiangiogenic property of pigment epithelium-derived factor in hepatocellular carcinoma. Hepatology 40: 252-259, 2004.
9. Maeshima Y, Colorado PC, Torre A, *et al*: Distinct antitumor properties of a type IV collagen domain derived from basement membrane. J Biol Chem 275: 21340-21348, 2000.
10. Maeshima Y, Yerramalla UL, Dhanabal M, *et al*: Extracellular matrix-derived peptide binds to alpha(v)beta(3) integrin and inhibits angiogenesis. J Biol Chem 276: 31959-31968, 2001.
11. Maeshima Y, Manfredi M, Reimer C, *et al*: Identification of the anti-angiogenic site within vascular basement membrane-derived tumstatin. J Biol Chem 276: 15240-15248, 2001.
12. Bergers G and Benjamin LE: Tumorigenesis and the angiogenic switch. Nat Rev Cancer 3: 401-410, 2003.
13. Hutchings H, Ortega N and Plouet J: Extracellular matrix-bound vascular endothelial growth factor promotes endothelial cell adhesion, migration, and survival through integrin ligation. FASEB J 17: 1520-1522, 2003.
14. Hamano Y and Kalluri R: Tumstatin, the NC1 domain of alpha3 chain of type IV collagen, is an endogenous inhibitor of pathological angiogenesis and suppresses tumor growth. Biochem Biophys Res Commun 333: 292-298, 2005.
15. Sund M, Hamano Y, Sugimoto H, *et al*: Function of endogenous inhibitors of angiogenesis as endothelium-specific tumor suppressors. Proc Natl Acad Sci USA 102: 2934-2939, 2005.
16. Cai J, Ahmad S, Jiang WG, *et al*: Activation of vascular endothelial growth factor receptor-1 sustains angiogenesis and Bcl-2 expression via the phosphatidylinositol 3-kinase pathway in endothelial cells. Diabetes 52: 2959-2968, 2003.
17. Abid MR, Guo S, Minami T, *et al*: Vascular endothelial growth factor activates PI3K/Akt/forkhead signaling in endothelial cells. Arterioscler Thromb Vasc Biol 24: 294-300, 2004.
18. Wu LW, Mayo LD, Dunbar JD, *et al*: Utilization of distinct signaling pathways by receptors for vascular endothelial cell growth factor and other mitogens in the induction of endothelial cell proliferation. J Biol Chem 275: 5096-5103, 2000.
19. Hamano Y, Zeisberg M, Sugimoto H, *et al*: Physiological levels of tumstatin, a fragment of collagen IV alpha3 chain, are generated by MMP-9 proteolysis and suppress angiogenesis via alphaV beta3 integrin. Cancer Cell 3: 589-601, 2003.
20. Mayoral R, Fernandez-Martinez A, Bosca L and Martin-Sanz P: Prostaglandin E2 promotes migration and adhesion in hepatocellular carcinoma cells. Carcinogenesis 26: 753-761, 2005.
21. Nejjari M, Hafdi Z, Gouysse G, *et al*: Expression, regulation, and function of alpha V integrins in hepatocellular carcinoma: an *in vivo* and *in vitro* study. Hepatology 36: 418-426, 2002.
22. Pasco S, Ramont L, Venteo L, Pluot M, Maquart FX and Monboisse JC: *In vivo* overexpression of tumstatin domains by tumor cells inhibits their invasive properties in a mouse melanoma model. Exp Cell Res 301: 251-265, 2004.
23. Maeshima Y, Sudhakar A, Lively JC, *et al*: Tumstatin, an endothelial cell-specific inhibitor of protein synthesis. Science 295: 140-143, 2002.
24. Sudhakar A, Sugimoto H, Yang C, Lively J, Zeisberg M and Kalluri R: Human tumstatin and human endostatin exhibit distinct antiangiogenic activities mediated by alpha v beta 3 and alpha 5 beta 1 integrins. Proc Natl Acad Sci USA 100: 4766-4771, 2003.
25. Kalluri R: Basement membranes: structure, assembly and role in tumour angiogenesis. Nat Rev Cancer 3: 422-433, 2003.
26. Bagli E, Stefaniotou M, Morbidelli L, *et al*: Luteolin inhibits vascular endothelial growth factor-induced angiogenesis; inhibition of endothelial cell survival and proliferation by targeting phosphatidylinositol 3'-kinase activity. Cancer Res 64: 7936-7946, 2004.
27. Hood JD, Frausto R, Kiosses WB, Schwartz MA and Cheresh DA: Differential alphav integrin-mediated Ras-ERK signaling during two pathways of angiogenesis. J Cell Biol 162: 933-943, 2003.

Clinicopathological study of hepatocellular carcinoma with peliotic change

MASARU FUJIMOTO[1,2], OSAMU NAKASHIMA[1], MINA KOMUTA[1], TOSHIMITSU MIYAAKI[1], MASAMICHI KOJIRO[1] and HIROHISA YANO[1]

[1]Department of Pathology, Kurume University School of Medicine, Kurume, Fukuoka 830-0011; [2]Division of Hepatology and Metabolism, Department of Internal Medicine, Faculty of Medicine, Saga University, Nabeshima 849-8501, Japan

Received May 25, 2009; Accepted September 23, 2009

DOI: 10.3892/ol_00000003

Abstract. Peliosis hepatis-like blood-filled cavities are frequently observed in the tumors of hepatocellular carcinoma (HCC). This finding is generally referred to as 'peliotic change' in HCC. However, the clinicopathological features of HCC with peliotic change (PHCC) are not fully understood. These issues are addressed in the present study. Among 294 consecutively surgically resected HCCs, the clinicopathological features of PHCC were compared with those of a common type of HCC (control). PHCC was observed in 116 (39.5%) of 294 HCCs. The mean tumor diameter of 3.4±0.9 cm of the PHCC group was significantly larger than that of the 2.5±0.9 cm of the control, and the incidence of PHCC was related to increased tumor diameter. In the 116 PHCCs, the tumors were completely or incompletely encapsulated. On ultrasonography, PHCCs showed hyperechoic and/or mosaic patterns. The mean diameter of 3.5±0.8 cm of PHCCs with a hyperechoic and/or mosaic pattern was significantly larger than that of 2.3±0.9 cm in the control. In conclusion, it is necessary for clinicians and pathologists to discern the characteristics of peliotic change as a morphological feature that modifies ultrasound findings.

Introduction

Peliosis hepatis, a hepatic lesion characterized by blood-filled parenchymal cavities randomly scattered throughout the liver (1-3), was first described by Wagner (4), but its pathogenesis is a matter of debate. Peliosis hepatis-like blood-filled cavities are also frequently observed in the tumors of hepatocellular carcinoma (HCC) (5-7). This finding is generally referred to as 'peliotic change' in HCC. Almost no clinicopathological assessment of this peliotic change has been conducted, and it is still considered little more than an often observed incidental or accidental finding. However, along with the advances in diagnostic imaging, peliotic change has drawn attention as a morphological feature that modifies image findings of HCC.

In the present study, we conducted a clinicopathological study of HCC with peliotic change (PHCC).

Materials and methods

A total of 294 HCCs without preoperative anticancer therapies were consecutively resected at Kurume University Hospital between January 1991 and December 2003. Cases showing a peliosis hepatis-like change (peliotic change) in the tumor were included for the study as PHCC and compared with cases of a common type of HCC as control. The resected liver specimens were fixed in 10% buffered formalin immediately after hepatectomy, cut serially into 5 mm slices and macroscopically examined. Sections containing tumor tissues as well as the surrounding liver tissues were embedded in paraffin, cut into 4-μm sections and routinely stained with hematoxylin and eosin. Immunohistochemical staining of CD34 was performed on 20 PHCC cases to examine the endothelial cells of the sinusoidal blood spaces of the tumor, using mouse monoclonal antibody against CD34 (anti-CD34; Dako, CA, USA) and the Streptavidin Peroxidase technique (MaxiTags kits, Immunon™, Lipshaw, PA, USA). Clinical data were obtained from clinical charts. Informed consent was obtained from the patients included in the study.

Statistical analysis was performed using Stat View version J-5.0 (Abacus Concepts Inc., Berkeley, CA, USA). Difference of means was assessed by the unpaired Student's t-test or Mann-Whitney U test. $P<0.05$ was considered statistically significant.

Results

Clinical findings of PHCC. PHCC was observed in 116 (39.5%) out of 294 cases. Ages ranged from 41 to 78 years (mean 63.2±7.8 SD) in the PHCCs and from 16 to 80 years (mean 64.5±8.8 SD) in the control group. The PHCC group

Correspondence to: Dr Hirohisa Yano, Department of Pathology, Kurume University School of Medicine, 67 Asahi-machi, Kurume, Fukuoka 830-0011, Japan
E-mail: hiroyano@med.kurume-u.ac.jp

Key words: hepatocellular carcinoma, peliotic change, peliosis hepatis, ultrasound, mosaic pattern

Table I. Comparison of the ultrasonographic pattern between hepatocellular carcinoma with peliotic change and a common type of HCC (control) according to the tumor size.

Tumor size (cm)	0.0-1.0	1.1-2.0	2.1-3.0	3.1-4.0	4.1-5.0	Total (%)
PHCC group						
Hyperechoic	0	0	3	5	4	12 (20)
Mosaic	0	1	7	5	5	18 (31)[a]
Isoechoic	0	2	2	2	2	8 (14)
Hypoechoic	0	4	7	10	0	21 (36)
Total	0	7	19	22	11	59 (100)
Control group						
Hyperechoic	3	7	6	1	0	17 (19)
Mosaic	0	3	6	1	1	11 (13)
Isoechoic	2	3	6	5	2	18 (20)
Hypoechoic	2	17	19	4	0	42 (48)
Total	7	30	37	11	3	88 (100)

[a]P<0.01 vs. mosaic in control.

included 89 males and 27 females (3.3:1), while the control group comprised 140 males and 38 females (3.7:1). No significant difference was noted in gender between the two groups.

Hepatitis B surface antigen (HBsAg) was found to be positive in 16 cases (15%) out of 104 in the PHCC group and in 20 cases (12%) out of 163 in the control group. Hepatitis C virus antibody (HCVAb) was found to be positive in 82 cases (77%) out of 107 in the PHCC group and in 132 cases (80%) out of 166 cases in the control group, indicating no significant difference between the two groups. In the remaining 27 and 21 of the 294 cases, respectively, HBsAg- and HCVAb-positives were unknown.

The laboratory data for asparate aminotransferase, alanine aminotransferase, albumin, as well as platelet and serum α-fetoprotein were not significantly different between the two groups.

Imaging findings of PHCC. Among 59 PHCCs in which abdominal ultrasound findings were available, 12 (20%) had a hyperechoic pattern and 18 (31%) a mosaic pattern. Among 88 cases of the control group, 17 (19%) had a hyperechoic pattern and 11 (13%) a mosaic pattern, indicating significantly more lesions with a mosaic pattern in the PHCC group (P<0.01; Table I). Furthermore, the mean tumor diameter in the cases with a hyperechoic pattern and/or mosaic pattern was 3.5±0.8 cm in the PHCC group and 2.3±0.9 cm in 28 controls. The tumor size of PHCCs with hyperechoic and/or mosaic patterns was significantly larger than that of the control (P<0.001).

In the majority of 50 cases in the PHCC group that underwent dynamic CT scans, typical HCC patterns were observed, such as high attenuation in the early enhanced phase and wash-out in the delay enhanced phase. No specific difference in CT findings was noted in PHCCs.

Pathological findings of PHCC. Tumor diameter ranged from 1.5 to 5.0 cm (average 3.4±0.9 SD) in the PHCC group and from 0.7 to 4.8 cm (average 2.5±0.9 SD) in the control group, indicating significantly larger tumors in the PHCC group (P<0.001; Table II). The incidence of PHCC was related to the increase of tumor diameter. Tumors <2 cm were found in 10 cases (9%) in the PHCC group and in 65 cases (37%) in the control. No tumors <1 cm in diameter were detected in the PHCC group.

Table II. Comparison in tumor size between hepatocellular carcinoma with peliotic change and a common type of HCC (control).

Tumor size (cm) Average ± SD	PHCC (%) 3.4±0.9[a]	Control (%) 2.5±0.9
0.0-1.0	0 (0)	11 (100)
1.1-2.0	10 (16)	54 (84)
2.1-3.0	37 (32)	77 (68)
3.1-4.0	44 (61)	28 (39)
4.1-5.0	25 (76)	8 (24)
Total	116 (100)	178 (100)

[a]P<0.001 vs. control.

The tumors were completely encapsulated in 108 (93%) of the 116 PHCCs, but incompletely encapsulated in the remaining 8 cases. On the other hand, encapsulated HCC was observed in 106 (60%) out of 178 tumors in the control group, indicating a significantly higher frequency of encapsulation in the PHCC group (P<0.001). Peliotic change was observed as varying sized blood lakes and hemorrhagic honeycomb-like appearance (Fig. 1A and B). In some cases, peliotic changes occupied ~2/3 of the cut surface of the tumor. Peliotic changes were easily distinguished from hemorrhage because the latter was accompanied by degeneration and/or necrosis of the tumor

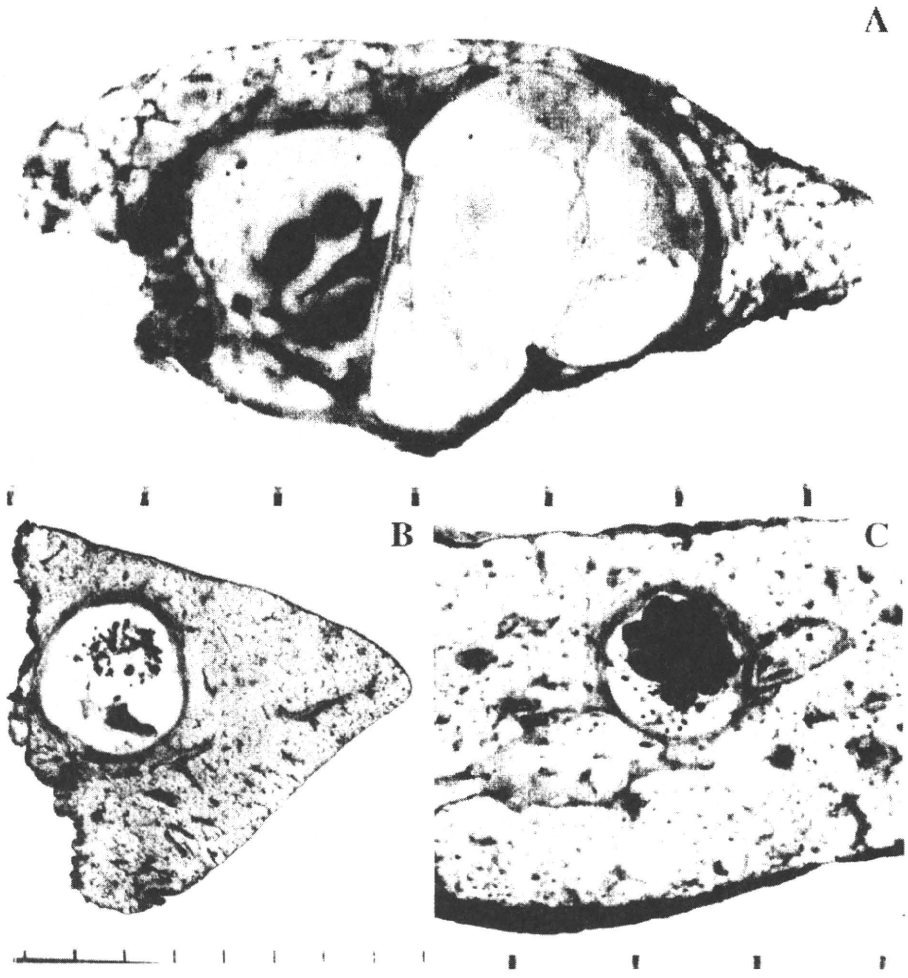

Figure 1. Macroscopic features of HCC with peliotic changes. (A) Dot-like peliotic changes. (B) Honeycomb-shaped and small blood lake-like peliotic changes in encapsulated tumor. (C) Blood lake-like peliotic change with clear boundaries occupying ~2/3 of the cut surface of the tumor.

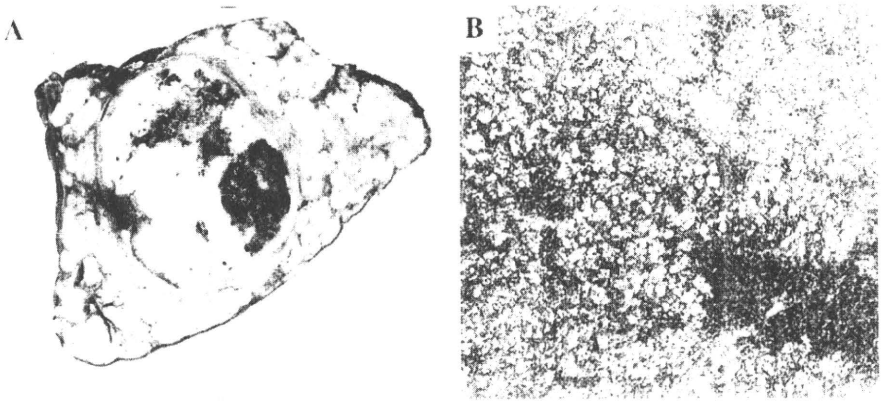

Figure 2. Hemorrhage in HCC. (A) Hemorrhage is observed in the degenerative and necrotic areas of the tumor. (B) Histologically diffuse hemorrhage is observed in degenerative HCC tissue.

tissue (Fig. 2). Fibrous septa were observed in 76 PHCCs (68%) and in 112 cases (63%) in the control group.

Peliotic change was observed as varying sized blood lakes without obvious lining of the endothelial cells (Fig. 3A). The lack of endothelial cells was also confirmed by immunostaining for CD34 (Fig. 3B). The majority of PHCCs were moderately differentiated showing a trabecular or pseudoglandular or both patterns. No well-differentiated type was found. Degeneration